J. Fluid Mech. (1999), *vol.* 395, *pp.* 125–159. Printed in the United Kingdom

© 1999 Cambridge University Press

The effect of weak shear on finite-amplitude internal solitary waves

By S. R. CLARKE AND R. H. J. GRIMSHAW

Department of Mathematics and Statistics, Monash University, Clayton, Vic. 3168, Australia

(Received 28 July 1998 and in revised form 21 April 1999)

A finite-amplitude long-wave equation is derived to describe the effect of weak current shear on internal waves in a uniformly stratified fluid. This effect is manifested through the introduction of a nonlinear term into the amplitude evolution equation, representing a projection of the shear from physical space to amplitude space. For steadily propagating waves the evolution equation reduces to the steady version of the generalized Korteweg–de Vries equation. An analysis of this equation is presented for a wide range of possible shear profiles. The type of waves that occur is found to depend on the number and position of the inflection points of the representation of the shear profile in amplitude space. Up to three possible inflection points for this function are considered, resulting in solitary waves and kinks (dispersionless bores) which can have up to three characteristic lengthscales. The stability of these waves is generally found to decrease as the complexity of the waves increases. These solutions suggest that kinks and solitary waves with multiple lengthscales are only possible for shear profiles (in physical space) with a turning point, while instability is only possible if the shear profile has an inflection point. The unsteady evolution of a periodic initial condition is considered and again the solution is found to depend on the inflection points of the amplitude representation of the shear profile. Two characteristic types of solution occur, the first where the initial condition evolves into a train of rank-ordered solitary waves, analogous to those generated in the framework of the Korteweg–de Vries equation, and the second where two or more kinks connect regions of constant amplitude. The unsteady solutions demonstrate that finite-amplitude effects can act to halt the critical collapse of solitary waves which occurs in the context of the generalized Korteweg–de Vries equation. The two types of solution are then used to qualititatively relate previously reported observations of shock formation on the internal tide propagating onto the Australian North West Shelf to the observed background current shear.

1. Introduction

While the dynamics of nonlinear internal solitary waves in the ocean are determined by a range of effects, many field observations indicate that vertical shear of the horizontal current is often one of the most significant. An important generation mechanism for nonlinear internal waves is the interaction of barotropic tides with topography. Here large-amplitude waves and shock-like structures with wavelengths of order hundreds of metres have been observed propagating on internal tides with wavelengths of order tens of kilometres. Observations of nonlinear internal waves due to this mechanism have been documented by, among others, Halpern (1971), Apel

https://doi.org/10.1017/S002211209900587X Published online by Cambridge University Press

et al. (1975), Farmer & Smith (1978), Haury, Briscoe & Orr (1979) and Holloway (1984, 1987, 1994). These show that in many circumstances current shear is sufficiently strong that it cannot be ignored, including circumstances where the shear is significantly smaller than the velocities associated with the internal waves. Farmer (1978) documents observations of nonlinear internal waves in a lake generated by a similar mechanism of the interaction of a storm surge with a sill. These also show the presence of significant background shear.

It was first shown by Benney (1966) that the propagation of long, weakly nonlinear internal waves is governed by the Korteweg–de Vries (KdV) equation:

$$A_t + cA_x + rAA_x + sA_{xxx} = 0, \tag{1}$$

where c is the linear long-wave speed, and r and s are coefficients dependent on the ambient stratification of the fluid. The derivation assumes that the leading-order balance is between the first two terms, and that nonlinearity and dispersion balance at the next order. Therefore, if a wave has characteristic amplitude a, the characteristic wavelength will be $\lambda = O((s/ra)^{1/2})$. Hence, if $ra \ll 1$ nonlinearity and dispersion will be weak effects. Motivated by the observations of internal wave generation in Massachusetts Bay by Halpern (1971), Lee & Beardsley (1974) used Benney's formulation to examine the effects of current shear, so that in the KdV equation (1) the parameters r and s become dependent on the shear as well as the stratification. This was further extended by Maslowe & Redekopp (1980), Grimshaw (1981), Tung, Ko & Chang (1981) and Gear & Grimshaw (1983) resulting in various modifications to (1). The derivations of Maslowe & Redekopp (1980) and Tung *et al.* (1981) demonstrated that not only is the evolution of regular internal wave modes governed by (1), the evolution of singular internal wave modes having a nonlinear-dominated critical layer where the phase speed of the internal wave equals that of the current shear are also governed by this equation. As noted by Tung *et al.* (1981) in this weakly nonlinear limit for regular modes and singular modes with nonlinear critical layers the effect of shear is purely kinematic, i.e. the shear only modifies the wave form and wave speed and there is no exchange of energy and momentum between the waves and the shear. The behaviour of the phase speed c and the coefficients r and s for various shear and stratification combinations is considered by Maslowe & Redekopp (1980), Tung *et al.* (1981), Gear & Grimshaw (1983), Smyth & Holloway (1988) and Holloway *et al.* (1997).

The customary ordering for weakly nonlinear waves is that $r = O(1)$ and $a \ll 1$. But if $r \approx 0$ the derivation of the KdV equation needs to be continued to a higher order of nonlinearity, and typically a modified KdV (mKdV) equation is obtained which contains a cubic nonlinear term. However, for a uniformly stratified Boussinesq fluid and no current shear this kind of nonlinearity vanishes to all orders. In this circumstance it is possible to remove the hypothesis of weak nonlinearity, and instead derive an evolution equation for finite-amplitude waves. Indeed, for the steady flow of a uniformly stratified Boussinesq fluid the fully nonlinear equations become linear (Dubreil-Jacotin 1937; Long 1953), and can thus be exploited to obtain exact analytical solutions. More generally, for a steady non-Boussinesq fluid this situation occurs when the upstream potential energy and kinetic energy are constant with depth. Benney & Ko (1978) studied the steady propagation of internal waves in a stratified fluid contained between rigid boundaries using the Dubreil-Jacotin equation. They made the long-wave approximation and showed that analytical solutions for exponential and linear stratifications could be obtained when the Boussinesq parameter is sufficiently small. This was extended

https://doi.org/10.1017/S002211209900587X Published online by Cambridge University Press

by Grimshaw & Yi (1991), who considered the resonant forcing of waves by the uniform flow of a stratified fluid past topography. Their formulation allowed for slow temporal variations, weak perturbations from uniform stratification, a small Boussinesq parameter and the presence of a free upper boundary. The amplitude of the internal wave was shown to satisfy an integro-differential evolution equation, which is highly nonlinear and, in general, must be solved numerically. This type of evolution equation is referred to as finite-amplitude long-wave (FALW) equation.

The derivation of FALW equations is not limited to stratified fluids, although in each case when FALW equations can be derived the circumstances are limited to anomalous, but important, special cases. For example, Benney (1979) considered the propagation of steady, barotropic Rossby waves on a weakly sheared zonal flow. This was extended by Warn (1983) to waves with temporal variations, and by Grimshaw & Yi (1993*a*) to the forcing of Rossby waves by topography. Other examples have been considered by Grimshaw & Yi (1990) for the propagation of barotropic coastally trapped waves and Grimshaw & Yi (1993*b*) for the propagation of inertial waves in a rotating cylinder.

Holloway (1984, 1987) documented the formation of internal hydraulic jumps and undular bores in the presence of current shear as the semidiurnal tide propagated onto the Australian North West Shelf, where the magnitude of the shear is small compared to the velocities associated with the internal tide. This was analysed by Smyth & Holloway (1988) using the second-order theory for nonlinear waves of Gear & Grimshaw (1983). They concluded that the steepening of the internal tide was strongly influenced by the background shear flow. Two shocks (i.e. internal hydraulic jumps) were reported as the tide propagated up the shelf, one forward breaking and the second rearward breaking. The first of these was trailed by a number of large-amplitude solitary waves. Smyth & Holloway (1988) were able to explain the presence of the first shock and argued that this would form into an undular bore. However, only a qualitative explanation of why the second shock may have formed could be given. A possible explanation for this inability to fully explain the second shock is found by considering the amplitudes of the waves, which were $O(40\,\mathrm{m})$ in water of depth $O(120\,\mathrm{m})$, so that the waves were certainly finite-amplitude in nature. Since the measurements of Holloway (1987) show that the background buoyancy frequency is approximately constant, while the magnitude of the background shear is relatively small, we suggest that features of this flow may be explained using a FALW theory.

Although FALW equations for stratified fluids are of limited application, they do allow a semi-analytical investigation of finite-amplitude effects. Here we use FALW equations to investigate the effect of shear on internal waves, where, due to the limitations of the theory, this shear must be weak in comparison with the velocities associated with the wave. The purpose of this study is, first, to gain a basic understanding of the effect of shear on finite-amplitude internal waves, and secondly, to attempt to explain the observations of internal waves reported by Holloway (1984, 1987). The structure of the paper is as follows. In § 2 the evolution equation describing the effect of weak shear on finite-amplitude internal waves is derived. In § 3 the structure and stablity of steady solutions of this equation are discussed, while in § 4 the evolution of periodic waves for various basic state parameters is investigated. These solutions are discussed in relation to the field observations of Holloway (1984, 1987) in § 5. The results are summarized in § 6.

https://doi.org/10.1017/S002211209900587X Published online by Cambridge University Press

2. Derivation of the evolution equation

We consider, following Grimshaw & Yi (1991), the inviscid, non-diffusive, two-dimensional propagation of long, finite-amplitude internal waves in a stratified fluid in a channel of undisturbed, constant depth h. Let the waves be characterized by a lengthscale L such that $L \gg h$. Thus we can define the small parameter

$$\epsilon = \frac{h^2}{L^2} \ll 1. \tag{2}$$

A Cartesian coordinate system $(x^*, z^*) = h(\epsilon^{-1/2}x, z)$ is introduced, where x^* is the horizontal coordinate along the duct and z^* is the vertical coordinate, increasing from zero at the base of the channel. The density is $\rho_0\rho(z-\zeta)$ where ζ is the dimensionless vertical particle displacement. The Boussinesq parameter, which measures the strength of the density stratification, is defined as

$$\beta = \rho(0) - \rho(1). \tag{3}$$

The reduced gravity is then $g' = \beta g$, where g is the magnitude of acceleration due to gravity. The fluid is assumed to be uniformly stratified, or close to uniform stratification, thus the normalized buoyancy frequency, N, is

$$N^2(z-\zeta) = -\frac{1}{\beta\rho}\frac{\mathrm{d}\rho}{\mathrm{d}z} = 1 + O(\beta). \tag{4}$$

The time variable is $t^* = (h/g'\epsilon)^{1/2}t$, while the fluid velocities are $(u^*, w^*) = (g'h)^{1/2}(u, \epsilon^{1/2}w)$. Further, it is assumed that the waves are of finite amplitude and the unperturbed fluid is weakly sheared, i.e. the imposed shear and its vertical derivative have magnitude $O(\epsilon)$. This latter condition effectively controls the magnitude of ϵ. Therefore, we write the velocities in terms of a perturbation streamfunction, ψ, and a mean flow, where

$$(u, w) = (\psi_z + \epsilon\bar{u}(z), -\psi_x), \tag{5}$$

and the subscripts denote partial differentation with respect to the appropriate variable. The perturbation vorticity, $-q$, is then

$$q = \psi_{zz} + \epsilon\psi_{xx}. \tag{6}$$

Finally, it is assumed here that $\beta \ll \epsilon$, and therefore, to the order considered we can set $\beta = 0$. Consequently, in this Boussinesq limit the dynamic upper boundary condition reduces to the rigid lid boundary condition. The following derivation can also be undertaken for small but finite β of $O(\epsilon)$, in which case extra nonlinear terms are added to the final evolution equation. These Boussinesq terms are identical to those for the equivalent derivation for an unsheared flow in Grimshaw & Yi (1991). We shall give only a brief outline of the derivation of the evolution equation here, as it is analogous to the Boussinesq case with zero background shear considered by Grimshaw & Yi (1991)

The long, finite-amplitude, unimodal waves propagate with a phase speed c and the changes in this frame of reference moving with the waves occur over a slow lengthscale $O(\epsilon x)$. Therefore, x and t are replaced by a phase and long space variable, defined as

$$\theta = \frac{x}{c} - t, \tag{7}$$

$$\chi = \epsilon x, \tag{8}$$

https://doi.org/10.1017/S0022112099005877X Published online by Cambridge University Press

while a streamfunction based coordinate is defined as

$$\xi = z - \frac{\psi}{c}. \tag{9}$$

Thus lines of constant ξ correspond to leading order to streamlines. The vorticity and density equations can now be written as

$$J\left(q + \frac{\psi}{c^2}, \xi\right) + \frac{1}{c}\left(\zeta - \frac{\psi}{c}\right)_\theta + \epsilon\left(-I(\psi_{zz}, \psi) - \frac{\bar{u}\psi_{zz\theta}}{c} + \frac{\bar{u}_{zz}\psi_\theta}{c} + \zeta_\chi\right) = O(\epsilon^2), \tag{10a}$$

$$J\left(\zeta - \frac{\psi}{c}, \xi\right) - \epsilon\left(I(\zeta, \psi) + \psi_\chi + \frac{\bar{u}\zeta_\theta}{c}\right) = O(\epsilon^2). \tag{10b}$$

with

$$\psi = 0 \quad \text{on} \quad z = 0, 1. \tag{10c}$$

The Jacobians in the above equations have the definition

$$J(a, b) \equiv a_\theta b_z - a_z b_\theta, \tag{11}$$

$$I(a, b) \equiv a_\chi b_z - a_z b_\chi \tag{12}$$

and now

$$q = \psi_{zz} + \frac{\epsilon\psi_{\theta\theta}}{c^2} + O(\epsilon^2). \tag{13}$$

These equations are transferred from (θ, z, χ)-space to (θ, ξ, χ)-space, which is valid so long as the transformation is one-to-one and $\xi_z \neq 0$. Therefore, the streamfunction must satisfy $|\psi_z| < c$; if $|\psi_z| = c$ a stagnation point (in the reference frame of the wave) will occur in the fluid, and subsequent to that overturning may occur. Then

$$J(a, \xi) = \xi_z a_\theta. \tag{14}$$

Integrating the equations of conservation of vorticity, (10*a*), and density, (10*b*), we can show that

$$\psi_{zz} + \frac{\psi}{c^2} + \epsilon\left(\frac{\psi_{\theta\theta}}{c^2} - G\right) = O(\epsilon^2), \tag{15a}$$

$$\zeta - \frac{\psi}{c} - \epsilon\int_\infty^\theta \frac{1}{\xi'_z}\left(\psi'_\chi + \frac{\bar{u}'\zeta'_\theta}{c} + I(\zeta', \psi')\right) \mathrm{d}\theta' = O(\epsilon^2), \tag{15b}$$

where

$$G = \int_\infty^\theta \left[\frac{1}{\xi'_z}\left(-\zeta'_\chi + \frac{\bar{u}'\psi'_{zz\theta}}{c} - \frac{\bar{u}'_{zz}\psi'_\theta}{c} + I(\psi'_{zz}, \psi')\right) - \frac{1}{c(\xi'_z)^2}\left(\psi'_\chi + \frac{\bar{u}'\zeta'_\theta}{c} + I(\zeta', \psi')\right)\right.$$
$$\left. - \frac{\xi'_\theta}{c\xi'_z}\frac{\partial}{\partial\xi}\int_\infty^{\theta'} \frac{1}{\xi''_z}\left(\psi''_\chi + \frac{\bar{u}''\zeta''_\theta}{c} + I(\zeta'', \psi'')\right) \mathrm{d}\theta''\right] \mathrm{d}\theta'. \tag{15c}$$

The primes denote the first argument of the various functions, e.g. $\psi'' = \psi(\theta'', \xi, \chi)$. Note that integration with respect to θ occurs along lines of constant ξ, i.e. streamlines. Here we are assuming that $\psi, \zeta \to 0$ as $\theta \to \infty$, since the linear spectrum indicates that there can be no waves ahead of the solitary wave. However, there will in general, be a trailing shelf of $O(\epsilon)$ which carries $O(1)$ mass (see Prasad & Akylas 1997). Fortunately, the details of this trailing shelf do not affect the evolution at leading order.

https://doi.org/10.1017/S002211209900587X Published online by Cambridge University Press

We introduce asymptotic solutions for ψ and ζ of the form

$$\psi = \psi^{(0)} + \epsilon\psi^{(1)} + O(\epsilon^2). \tag{16}$$

At zeroth order

$$\psi^{(0)} = c^2 A(\theta, \chi)\phi(z), \quad \zeta^{(0)} = \frac{\psi^{(0)}}{c}, \tag{17a,b}$$

where

$$c = \frac{1}{n\pi}, \quad \phi = \sin n\pi z, \tag{17c,d}$$

and n is a non-zero positive integer. Hence, to leading order $z(\xi, A)$ is the solution of the implicit equation

$$\xi = z - \frac{A}{n\pi}\sin n\pi z, \tag{18}$$

and the condition $|\psi_z| < c$ implies the amplitude must satisfy

$$|A| < 1, \tag{19}$$

to prevent overturning. If $|A| > 1$, then it may be possible to construct a solitary wave solution with a vortex core, similar to that found by Derzho & Grimshaw (1997) for the case when $\bar{u}(z) \equiv 0$, but the $O(\beta)$ terms are retained.

At first order the compatability condition for the non-homogeneous boundary-value problem for $\psi^{(1)}$ requires that

$$\tfrac{1}{2}A_{\theta\theta} - \int_0^1 G^{(0)}\phi z_\xi \,\mathrm{d}\xi = 0, \tag{20a}$$

where

$$G^{(0)} = \int_\infty^\theta \left[-\frac{\phi'}{c\xi'_z}(c^2 A'_\chi + A'_\theta(\bar{u}' + c^2\bar{u}'_{zz})) - \frac{\phi'}{c(\xi'_z)^2}(c^2 A'_\chi + \bar{u}' A'_\theta) \right.$$
$$\left. + \frac{A'_\theta \phi'}{\xi'_z}\frac{\partial}{\partial\xi}\int_\infty^{\theta'} \frac{\phi''}{\xi''_z}(c^2 A''_\chi + \bar{u}'' A''_\theta)\,\mathrm{d}\theta'' \right] \mathrm{d}\theta'. \tag{20b}$$

It can then be shown that A satisfies the integro-differential equation

$$\frac{2}{c}\int_\infty^\theta K_n(A, A')A'_\chi \,\mathrm{d}\theta' + g(A) + A_{\theta\theta} = 0, \tag{21a}$$

where

$$K_n(A, A') = \int_0^1 \frac{\partial z}{\partial A}\left[\frac{\partial z'}{\partial A'}\left(1 + \frac{\partial z'}{\partial \xi}\right) - (z - z')\frac{\partial}{\partial\xi}\left(\frac{\partial z'}{\partial A'}\right)\right]\mathrm{d}\xi, \tag{21b}$$

$$g(A) = -2n\pi\int_0^1 \left(1 - \left(\frac{\partial z}{\partial\xi}\right)^2\right)\frac{\partial z}{\partial\xi}(\cos n\pi z - A)\,\bar{u}(\xi)\,\mathrm{d}\xi. \tag{21c}$$

As expected, the kernel $K_n(A, A')$ is identical to that obtained by Grimshaw & Yi (1991) for the case $\bar{u} = 0$ and $\beta \neq 0$. Note that as the shear is a weak effect, without loss of generality we can allow it to be a slowly varying function of χ. This introduces a mean vertical velocity, but as this will be $O(\epsilon^2)$, it does not affect the present analysis. Thus, the only consequence of this in (21) is that $g(A)$ will also become a slowly varying function of χ.

https://doi.org/10.1017/S002211209900587X Published online by Cambridge University Press

If $\bar{u}$ is constant in χ, an alternative formulation is to use a space-like phase variable and a long time variable, which are defined respectively as

$$\sigma = x - ct, \tag{22}$$

$$\tau = \epsilon t. \tag{23}$$

In this case (21) becomes

$$\frac{1}{c^2}\int_{\infty}^{\sigma} K_n(A, A')A'_{\tau}\,\mathrm{d}\sigma' + \frac{c}{2}g(A) + \frac{c^3}{2}A_{\sigma\sigma} = 0. \tag{24}$$

In the weakly nonlinear limit, $A = O(\epsilon)$, it can be shown that

$$K_n(A, A') = c^2 + O(\epsilon^2), \tag{25}$$

therefore, (24) becomes

$$A_{\tau} + 2\int_0^1 (1-\phi^2)\bar{u}\,\mathrm{d}zA_{\sigma} + 6c\int_0^1 (1-3\phi^2)\phi_z\bar{u}\,\mathrm{d}zAA_{\sigma} + \frac{c^3}{2}A_{\sigma\sigma\sigma} = O(\epsilon^3). \tag{26}$$

This is simply the KdV equation, which, taking into account the definition of A, can be shown to be in agreement with the KdV equations derived for weakly nonlinear waves in a sheared environment in the limit of uniform stratification and weak shear, e.g. see Grimshaw (1997).

The kernel in (21) can be shown to have a similarity form, dependent only on the modal number, n, through a multiplying factor. To demonstrate this, for a wave of mode n, where n is a positive integer, introduce the variables

$$(\hat{\xi}, \hat{z}) = n(\xi, z), \tag{27}$$

which satisfy

$$\hat{\xi} = \hat{z} - \frac{A}{\pi}\sin\pi\hat{z}. \tag{28}$$

Both $\hat{\xi}$ and $\hat{z}$ extend over the range $[0, n^{-1}]$, thus the vertical integrals must also be evaluated over this interval. It can be shown that

$$K_n(A, A') = (n\pi)^2\int_0^1 \frac{\partial\hat{z}}{\partial A}\left[\frac{\partial\hat{z}'}{\partial A'}\left(1 + \frac{\partial\hat{z}'}{\partial\hat{\xi}}\right) - (\hat{z} - \hat{z}')\frac{\partial}{\partial\hat{\xi}}\left(\frac{\partial\hat{z}'}{\partial A'}\right)\right]\mathrm{d}\hat{\xi},$$

$$= c^2K(A, A'). \tag{29}$$

Similarly the nonlinear term due to velocity shear is

$$g(A) = -2\pi\int_0^1 \left(1 - \left(\frac{\partial\hat{z}}{\partial\hat{\xi}}\right)^2\right)\frac{\partial\hat{z}}{\partial\hat{\xi}}(\cos\pi\hat{z} - A)\,\bar{u}_{eff}(\hat{\xi})\,\mathrm{d}\hat{\xi}, \tag{30a}$$

where

$$\bar{u}_{eff}(\hat{\xi}) = \sum_{k=0}^{n-1}\bar{u}\left[\frac{1}{n}(-1)^k\hat{\xi} + \frac{k}{n} - \frac{1}{2n}(1 - (-1)^k)\right]. \tag{30b}$$

Defining

$$\hat{\chi} = \frac{\chi}{2c}, \tag{31}$$

https://doi.org/10.1017/S0022112099005877X Published online by Cambridge University Press

and subsequently dropping the accent, (21) becomes

$$\int_{\infty}^{\theta} K(A, A')A'_{\chi}\,\mathrm{d}\theta' + g(A) + A_{\theta\theta} = 0. \tag{32}$$

Therefore higher modes, $n > 1$, see an effective velocity which is simply a smoothed form of the actual velocity. Henceforth we will confine our comments to mode 1 waves and drop the accents in (29) and (30).

The Richardson number in this flow is

$$Ri = \frac{N^2}{u_z^2} = (A\phi)^{-2} + O(\epsilon). \tag{33}$$

Therefore, the minimum Richardson number is

$$Ri \approx A^{-2}. \tag{34}$$

If the wave reaches the critical amplitude, $|A| = 1$, the minimum Richardson number is then $Ri \approx 1$ and occurs equidistant between the points of overturning.

3. Steady waves

For steady waves the nonlinear integro-differential equation (32) reduces to a second-order nonlinear ordinary differential equation. This simplification allows us to efficiently consider the effect of a wide class of shears. Therefore assume that steady solutions of (32) exist of the form

$$A = A(\theta - U\chi), \tag{35}$$

where U is a constant, and consequently $A_{\chi} = -UA_{\theta}$. Then, as

$$\int_{\infty}^{\theta} K(A, A')A'_{\theta'}\,\mathrm{d}\theta' = A, \tag{36}$$

equation (32) becomes

$$-UA + g(A) + A_{\theta\theta} = 0. \tag{37}$$

In deriving (32) it has been assumed that far upstream $A = 0$; however if the amplitude is constant but non-zero upstream, $A = A_0$ say, then it is obvious (37) should have a correction to the right-hand side. In this case

$$-UA + g(A) + A_{\theta\theta} = -UA_0 + g(A_0). \tag{38}$$

Now, following Warn (1983) a generalized dispersion relation for solitary wave solutions can be derived. The nonlinear function can be written as

$$g(A) - g(A_0) = (A - A_0)g'(A_0) + \alpha f(A, A_0), \tag{39}$$

where $f = O((A - A_0)^2)$ as $A \to A_0$ and α can always be chosen to be strictly positive. For a solitary wave to exist, $A \to A_0$ as $\theta \to \pm\infty$ and hence $U > g'(A_0)$. Introducing

$$V = \alpha^{-1}(U - g'(A_0)), \quad y = (\alpha V)^{1/2}\theta, \tag{40a,b}$$

equation (39) becomes

$$A_{yy} = A - A_0 - V^{-1}f(A, A_0). \tag{41}$$

https://doi.org/10.1017/S002211209900587X Published online by Cambridge University Press

Multiplying by A_y and integrating once gives

$$A_y^2 = (A - A_0)^2 - 2V^{-1} \int_{A_0}^{A} f(A', A_0)\, \mathrm{d}A'. \tag{42}$$

For a solitary wave with amplitude a at its extrema the dispersion relation is therefore

$$V(a, A_0) = \frac{2}{(a - A_0)^2} \int_{A_0}^{a} f(A', A_0)\, \mathrm{d}A'. \tag{43}$$

The velocity of the steady waves is then

$$U = \frac{2}{(a - A_0)^2} \int_{A_0}^{a} (g(A') - g(A_0))\, \mathrm{d}A'. \tag{44}$$

Since $\alpha > 0$ solitary waves can only exist for

$$V > 0, \tag{45}$$

and for each solitary wave

$$V(A, A_0) \leqslant V \text{ where } 0 \leqslant \operatorname{sgn}(a - A_0)(A - A_0) \leqslant |a - A_0|. \tag{46}$$

As the wave must satisfy the condition (19), solitary waves can only occur in the range

$$-1 < a, A_0 < 1. \tag{47}$$

Using these three conditions the function $V(a, A_0)$ can be plotted for each $g(A)$ to determine the types of solitary waves that are possible and the regions in which these occur. The forms of shear that need be considered can be reduced by noting that $g(A)$ is invariant under the transform

$$z \to 1 - z, \quad A \to -A. \tag{48}$$

Thus if the shear is reflected in the line $z = \frac{1}{2}$ the same solitary waves occur, but of opposite amplitude.

The stability of these solitary waves can be determined using the criteria derived by Pelinovsky & Grimshaw (1997). Defining the integral quantity

$$P^* = \int_{-\infty}^{\infty} (A - A_0)^2\, \mathrm{d}\theta, \tag{49}$$

they showed that solitary wave solutions of (32) are only stable when

$$\frac{\mathrm{d}P^*}{\mathrm{d}U} > 0. \tag{50}$$

Strictly this result was obtained for the case $A_0 = 0$, but we will use the more general form here. Using (42) and (43), it can be shown that

$$\frac{1}{2}\alpha^{1/2} P^* = \int_{A_0}^{a} \frac{(A - A_0)\, \mathrm{d}A}{(V - V(A, A_0))^{1/2}} = P. \tag{51}$$

Then the stability condition (50) is equivalent to

$$\frac{\mathrm{d}P}{\mathrm{d}V} > 0. \tag{52}$$

This stability result is uniformly valid for $K(A, A') \equiv 1$, i.e. when solutions of (38) are

https://doi.org/10.1017/S002211209900587X Published online by Cambridge University Press

steady solutions of the generalized KdV (gKdV) equation

$$A_\chi + g_A A_\theta + A_{\theta\theta\theta} = 0. \tag{53}$$

For a review of solitary wave instability in this context see Pelinovsky & Grimshaw (1996).

As an example, consider the stability of solitary waves for the nonlinearity

$$f = f_k (A - A_0)^k, \tag{54}$$

where k is a positive integer greater than unity. For $k \geqslant 5$ and odd Pelinovsky & Grimshaw (1997) showed that long internal solitary waves would be unstable. For general k

$$V = \frac{2 f_k}{k+1} (a - A_0)^{k-1}. \tag{55}$$

Thus, if k is even solitary waves can only occur if $f_k(a - A_0)$ is positive, and if k is odd solitary waves can only occur if f_k is positive. Then

$$P = \sigma V^{\frac{5-k}{2(k-1)}}, \tag{56}$$

where σ is some positive constant. Hence, for $k < 5$ solitary waves are stable, for $k = 5$ marginally stable and $k > 5$ unstable.

Next we consider the existence and stability of solitary waves when the shear is given by a quartic function of z,

$$\bar{u}(z) = \sum_{k=0}^{4} a_k z^k. \tag{57}$$

The coefficient a_0 can be arbitrarily chosen, therefore let

$$a_0 = -\frac{1}{2}\left(a_1 + \frac{2a_2}{3} + \frac{a_3}{2} + \frac{2a_4}{5}\right) - \frac{1}{4\pi^2}(2a_2 + 3a_3 + 4a_4) + \frac{3a_4}{2\pi^4}, \tag{58}$$

so that the coefficient of the linear term of g is zero. Then

$$g(A) = \sum_{k=2}^{5} g_k A^k, \tag{59a}$$

where

$$g_2 = -\frac{2}{\pi}(2a_1 + 2a_2 + 3a_3 + 4a_4) + \frac{56}{3\pi^3}(a_3 + 2a_4), \tag{59b}$$

$$g_3 = \frac{1}{2\pi}(2a_2 + 3a_3 + 4a_4) - \frac{3a_4}{4\pi^3}, \quad g_4 = -\frac{8}{3\pi^3}(a_3 + 2a_4), \quad g_5 = \frac{3a_4}{4\pi^3}, \tag{59c–e}$$

and the dispersion relation is

$$V = 2\sum_{k=2}^{5} \frac{g^{(k)}(A_0)(a - A_0)^{k-1}}{(k+1)!}, \tag{60}$$

where $g^{(k)}$ is the kth derivative of g.

When $\bar{u}(z)$ is just a quadratic function of z (i.e. $a_3 = a_4 = 0$), then $g_4 = g_5 = 0$ and so (41) reduces to the steady version of the mKdV equation. Its solitary wave solutions are well known and can be shown to be always stable. Let $a_3 = a_4 = 0$ in

https://doi.org/10.1017/S002211209900587X Published online by Cambridge University Press

(59), and define

$$\hat{a} = a - A_0, \quad r = g_2 + 3g_3A_0, \quad q = g_3. \tag{61}$$

Then setting $\alpha = 1$ the dispersion relation is

$$V = \tfrac{2}{3}r\hat{a} + \tfrac{1}{2}q\hat{a}^2. \tag{62}$$

The general solitary wave solution is (see Kakutani & Yamasaki 1978; Miles 1979)

$$A = A_0 + \frac{\hat{a}}{b + (1-b)\cosh^2 y/2}, \tag{63a}$$

where

$$b = -\frac{3q\hat{a}}{4r + 3q\hat{a}}. \tag{63b}$$

If $b \to 1$ kinks or dispersionless bores, i.e. solutions with unequal asymptotic limits as $y \to \pm\infty$, occur, where

$$A = A_0 + \tfrac{1}{2}\hat{a}(1 \pm \tanh y/2). \tag{64}$$

The stability of both the solitary waves and the kinks is then dependent on $P(A)$, given by

$$\begin{aligned} P &= \sqrt{2}\int_0^{\hat{a}} \frac{A\ \mathrm{d}A}{(q(\hat{a}^2 - A^2) + 4r(\hat{a} - A)/3)^{1/2}}, \\ &= \sqrt{2}|\hat{a}|\int_0^1 \frac{A\ \mathrm{d}A}{(1-A)^{1/2}(q(1+A) + 4r/(3\hat{a}))^{1/2}}. \end{aligned} \tag{65}$$

The form of (65) is dependent on the sign of q. For q positive first define

$$\mu = \frac{3q\hat{a}}{4r} + \frac{1}{2}, \tag{66}$$

and then the velocity can be written as

$$\frac{4V}{v} = 4\mu^2 - 1 = \hat{V}, \quad \text{where } v = \frac{8r^2}{9q}. \tag{67}$$

Note that since $V > 0$, $|\mu| \geqslant \frac{1}{2}$. It follows that

$$P = \left(\frac{v}{q^2}\right)^{1/2}\left(\hat{V}^{1/2} + \arctan \hat{V}^{-1/2} - \frac{\pi}{2}\operatorname{sgn}\mu\right), \tag{68}$$

and

$$\frac{\mathrm{d}P}{\mathrm{d}V} = \frac{2}{(vq^2)^{1/2}}\frac{\hat{V}^{1/2}}{1+\hat{V}}, \tag{69}$$

which is always positive. Thus for q positive the solitary waves are always stable.

For q negative

$$-\frac{4V}{v} = 1 - 4\mu^2 = \hat{V}, \tag{70}$$

so that now $|\mu| \leqslant \frac{1}{2}$. Then

$$P = \left|\frac{v}{q^2}\right|^{1/2}\left(-\hat{V}^{1/2} + \operatorname{arctanh}\hat{V}^{1/2}\right), \tag{71}$$

https://doi.org/10.1017/S002211209900587X Published online by Cambridge University Press

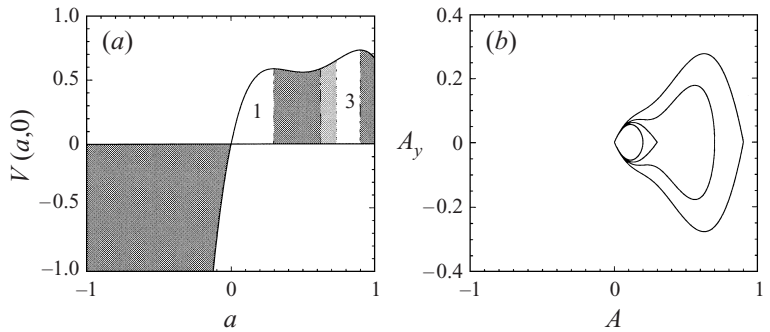


FIGURE 1. Examples of the possible types of solitary waves when the dispersion relation $V(a,0)$, (60), has g_5 negative and three positive turning points. (*a*) An example $V(a,0)$ showing the regions in which the various types of solitary waves occur. The types of solitary waves, indicated by a number, are discussed in the text. The regions in which solitary waves cannot occur are shown in dark shading, while the regions in which unstable solitary waves occur are shown in light shading. (*b*) Examples of phase plots of solitary waves from each of the regions of (*a*), including the limiting kink if it occurs.

and so

$$\frac{\mathrm{d}P}{\mathrm{d}V} = \frac{2}{|vq^2|^{1/2}} \frac{\hat{V}^{1/2}}{1-\hat{V}}, \tag{72}$$

which is always positive, since $\hat{V} < 1$. Thus, for q negative the solitary waves are again always stable.

The stability of kinks is found in the limit $\mu \to 0$. In this case P is only defined for q negative and

$$\lim_{\mu \to 0} \frac{\mathrm{d}P}{\mathrm{d}V} = \frac{2}{|vq^2|^{1/2}} \frac{1}{4\mu^2}. \tag{73}$$

Thus, kinks are stable in the sense that they are the limit as $\mu \to 0$ of stable solitary waves.

For the general case (57), the nonlinearity in (41) is of fifth order, and four types of curves for $V(a, A_0)$ are possible. These are dependent on the sign of the coefficient of the leading-order term of V and the distribution of the turning points on either side of $a = A_0$. From these four types of curves, four types of solitary waves result. Examples of phase plots of each of these types of solitary waves are shown in figures 1 and 2 for two of the possible types of curves for $V(a,0)$. The examples shown have $A_0 = 0$, for non-zero A_0 the same types of curves and solitary waves result, only the range of amplitudes over which these occur changes.

Figure 1 shows an example where type 1 and type 3 solitary waves and kinks are possible, and where regions of unstable solitary waves occur. The type 1 waves are all stable; however the type 3 solitary waves only stabilize as the amplitude increases. The limiting kinks occur at local maxima of V. Type 1 solitary waves are characterized by the behaviour that when plotted on a phase-plane, as in figure 1, the phase plots of all the type 1 solitary waves of the same family with smaller absolute amplitude will fall inside this curve. Thus, if a limiting kink exists the phase plots for the forward and backward facing waves form an envelope for the phase plots of the type 1 solitary waves. In the limit $|y| \to \infty$ these type 1 waves are subexponential, that is, coming inwards the waves decrease from exponential growth. The maximum growth rate of the wave, that is, the absolute maximum of $\mathrm{d}A_y/\mathrm{d}A$, occurs at $\pm\infty$ where $A = 0$. The

https://doi.org/10.1017/S002211209900587X Published online by Cambridge University Press

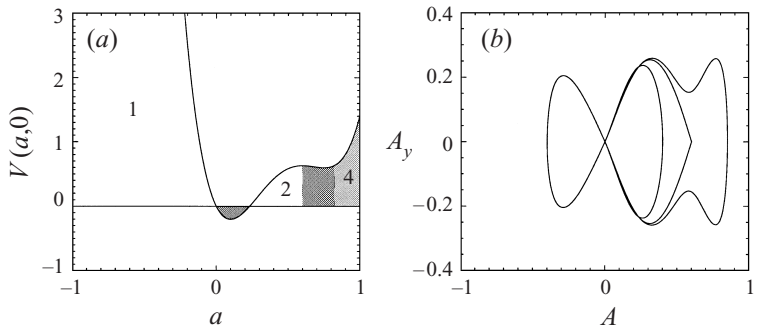


FIGURE 2. As for figure 1, except g_5 is positive.

solution (63) is an example of a type 1 solitary waves when $|b| \leqslant 1$. For type 3 waves to exist type 1 waves must occur at smaller absolute amplitudes. Type 3 waves are characterized by having two different lengthscales, or equivalently, two local maxima of their growth rate. This is more pronounced for smaller amplitudes where instability occurs.

For g_5 negative the existence conditions place a limit on the absolute amplitude of possible solitary waves. When g_5 is positive no such limit is imposed. In figure 2 an example of positive g_5 is shown where type 1, 2 and 4 solitary waves can occur, and a type 2 limiting kink occurs. The type 1 and 2 waves are all stable and the type 4 waves are all unstable. In contrast to type 1 waves, the phase plot for a type 2 solitary wave of a given amplitude no longer forms an envelope for the solitary waves of smaller absolute amplitude. The type 2 waves are superexponential in the limit $|y| \to \infty$, that is, the wave increases from exponential growth coming in towards the peak. In this case the maximum growth rate occurs away from $\pm\infty$ at non-zero A. When $b \leqslant -1$ the solution (63) is an example of a type 2 solitary wave. The limiting kink of the type 1 solitary waves is subexponential as $A \to 0$. For cubic nonlinearity this kink is also subexponential as $A \to a$. However, for higher-order nonlinearity this wave can be superexponential as $A \to a$. In this case a limiting kink for a family of type 1 solitary waves is also, under the correct transformation, the limiting kink for a family of type 2 solitary waves. For type 4 waves to exist type 2 waves must occur at smaller absolute amplitudes. The behaviour of type 4 waves is similar to that of type 3 waves, except that for small A the growth is superexponential. The two local maxima of the growth rate of the type 4 solitary wave shown in figure 2 are clearly apparent.

In figure 2 for large absolute values of a the quintic term in $g(A)$ dominates, which is known to be marginally stable. Therefore, in figure 2 for large positive a the solitary waves are unstable such that $\mathrm{d}P/\mathrm{d}V \to 0^-$, while for large negative a the solitary waves are stable such that $\mathrm{d}P/\mathrm{d}V \to 0^+$.

As the order of the shear and nonlinearity increases more types of solitary waves and kinks are possible; however as these solitary waves are dominated by higher-order nonlinearity, they will generally be unstable. Kinks though, where they exist, generally appear to be stable. It can be shown that a necessary condition for a type N solitary wave or a limiting type $N-1$ kink to exist is that the function $g(A)$ must have at least $N-1$ inflection points in the range $[-1, 1]$. Thus, a type N solitary wave or a type $N-1$ limiting kink requires at least $O(N+1)$ nonlinearity, or $O(N)$ shear, to occur.

https://doi.org/10.1017/S0022112099005877X Published online by Cambridge University Press

In figures 3–6 the regions of existence and stability of solitary waves are shown as a function of a and A_0 for four families of shear. We refer to these diagrams here as the characteristic diagram for the shear, or nonlinearity. Since

$$\lim_{a\to A_0} V(a, A_0) = \tfrac{1}{3}(a - A_0)g''(A_0), \tag{74}$$

the inflection points of g are apparent on these diagrams as the points at which $V(a, A_0)$ has a double root, that is, where the existence regions cross the line $a = A_0$. At these values of A_0 a change in the type of the solitary wave always occurs, although transitions can also occur at other values of A_0.

In figure 3 the characteristic diagram is shown for

$$\bar{u} = -\gamma\left(2z^3 - 3z^2 + \frac{28z}{3\pi^2}\right), \tag{75}$$

$$g = \frac{16\gamma A^4}{3\pi^3}. \tag{76}$$

Since g is even, identical waves occur for positive and negative γ. Here only type 1 solitary waves occur and these are unstable in a large region of the diagram. This contrasts with the results for the power law (54), for which instability only occurs for $k \geqslant 5$. However, here instability only occurs off the line $A_0 = 0$, which, in the context of the gKdV equation, corresponds to a mixed nonlinear term. If the coefficient of the linear term in (75) is decreased slightly the double inflection point of g vanishes, while the inflection point of $\bar{u}$ is unaffected. As the coefficient is increased further the regions of instability gradually recede away from the point $a = A_0 = 0$ and eventually disappear off the diagram. Compare this with cubic nonlinearity, with g_3 and g_2 such that g does not have an inflection point on $[-1, 1]$. In this case $\bar{u}$ also does not have an inflection point. The same types of waves result, but they are always stable.

If the linear coefficient in (75) is increased slightly the double inflection point of g separates into two distinct inflection points. An example is shown in figure 4, where

$$\bar{u} = -\gamma\left(2z^3 - 3z^2 + \left(\frac{3}{\pi}\right)^2 z\right), \tag{77}$$

$$g = \frac{4\gamma A^2}{3\pi^3}\left(4A^2 - 1\right). \tag{78}$$

Again identical types of waves occur for positive and negative γ. Type 1, 2 and 3 solitary waves occur, where the type 3 solitary waves are unstable for all possible amplitudes and the type 1 and 2 solitary waves are unstable in large regions outside the enclosed existence regions. The type 1 and 2 solitary waves which occur in the enclosed existence region are all stable. Typically, solitary waves which occur in such enclosed regions are found to be stable. Type 1 and 2 kinks now also occur on any horizontal line, i.e. line of constant A_0, where there is some finite region in which amplitudes are possible. The kinks occur at the limit of these regions furthest from the point $a = A_0$. Then as A_0 varies this gives a curve upon which kinks exist, referred to here as the kink curve(s). A continuum of 'kink pairs' can be constructed on these diagrams by drawing a rectangle with horizontal and vertical sides and vertices on the line $a = A_0$ and on the kink curve. An example is shown in figure 4. The resultant pair of kinks are then simply forward and rearward facing forms of the same wave. This pair takes the amplitude from A_0 to some amplitude a, where an arbitrary-length plateau can be inserted and then the rear kink returns the amplitude to A_0. In figure

https://doi.org/10.1017/S002211209900587X Published online by Cambridge University Press

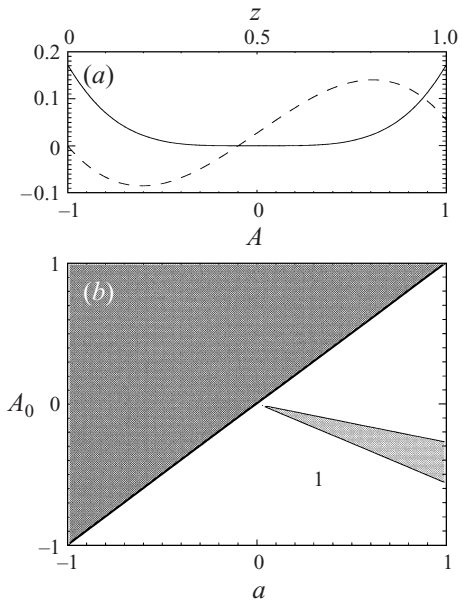


FIGURE 3. The regimes for the existence of stable and unstable solitary waves for the shear (75) and nonlinear function (76). (*a*) The shear $\bar{u}(z)$, shown as a dotted line, and the nonlinear function $g(A)$, shown as a solid line, for $\gamma = 1$. (*b*) The solitary wave regimes shown as a function of the amplitude, a, and the upstream level, A_0, for positive γ. For negative γ the characteristic diagram is simply rotated 180°. The regions in which solitary waves do not exist are shown in dark shading, while the regions in which unstable solitary waves occur are shown in light shading. Here the number 1 indicates only type 1 solitary waves occur.

4 kink pairs can join two type 1 kinks, in which case the rectangle spans only the lower inflection point, or a type 1 and a type 2 kink, in which case the rectangle spans both inflection points.

An example of quintic nonlinearity is shown in figure 5, where

$$\bar{u} = \gamma \left((z(1-z))^2 - \frac{3}{4\pi^2} z(1-z) \right), \tag{79}$$

$$g = \frac{3\gamma A^5}{4\pi^3}. \tag{80}$$

Here, for positive γ type 1 and 2 solitary waves occur: the former are all stable and the latter all unstable. For negative γ type 1 solitary waves and kinks occur, which are everywhere stable except in a small region near the origin. Here kink pairs can be constructed over the whole range of amplitudes. If the coefficient of the term $z(1-z)$ in (79) is decreased from $-\frac{3}{4}\pi^2$ the triple inflection point at $A = 0$ changes to a single inflection point. In this limit the regions of existence of solitary waves remain unchanged; however the regions of instability recede from the point $a = A_0 = 0$, eventually vanishing off the diagram. This limit corresponds to the inflection points of $\bar{u}$ moving closer together; however the instability regions have receded off the diagram well before the inflection points of $\bar{u}$ coalesce. Except for the large regions of instability in figure 5 these diagrams are very similar to the equivalent diagrams for purely cubic nonlinearity.

If the coefficient of the term $z(1-z)$ in (79) is increased from $-\frac{3}{4}\pi^2$ the triple

https://doi.org/10.1017/S002211209900587X Published online by Cambridge University Press

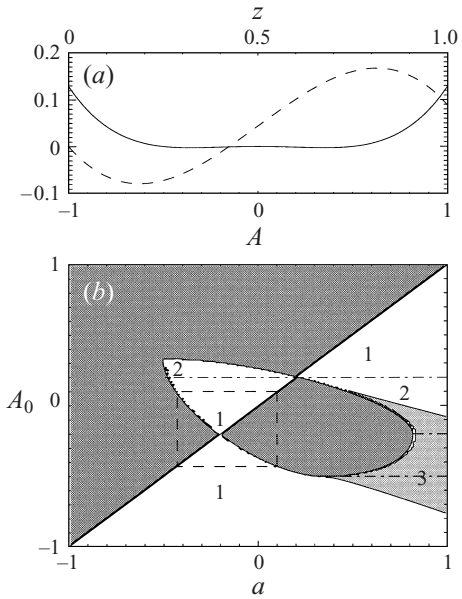


FIGURE 4. As for figure 3, except for the shear (77) and nonlinear function (78). Now more than one type of solitary wave can occur; the regions on the characteristic diagram where each type of solitary wave occurs is denoted by the appropriate number. The boundaries between the various regions are shown by a dashed-dotted line. Kinks can now also occur, an example of a kink pair is shown as a dashed line about the lower inflection point.

inflection point of g separates into three distinct inflection points. An example of this is shown in figure 6, where

$$\bar{u} = \gamma(z(1-z))^2, \tag{81}$$

$$g = \frac{3\gamma A^3}{4\pi^3}(A^2 - 1). \tag{82}$$

For positive and negative γ enclosed regions of type 1 and 2 solitary waves with limiting kinks occur which are completely stable. Type 1, 2, 3 and 4 solitary waves occur outside these regions for positive γ, where the type 3 and 4 solitary waves are completely unstable and the type 2 waves are only partially stable. Note that the type 3 regions, which are adjacent to the type 4 regions, are too small to show on the diagram. For negative γ type 1 and 3 solitary waves occur in the regions outside the enclosed existence regions. These regions all have limiting kinks, and thus are at least partially stable. The type 1 regions are almost completely stable. Kink pairs can be constructed for positive and negative γ, encompassing up to three inflection points. For positive γ all the kink pairs encompass the central inflection point. The kink pairs which encompass three inflection points join two type 2 kinks. For negative γ the kink pair encompassing three inflection points joins two type 1 kinks or two type 3 kinks.

For polynomial shear of higher order g can be evaluated using symbolic algebra packages; however for general shear profiles numerical integration must be used. In general though, a bound on g can be obtained and in two special cases approximate expressions for g can be found.

https://doi.org/10.1017/S002211209900587X Published online by Cambridge University Press

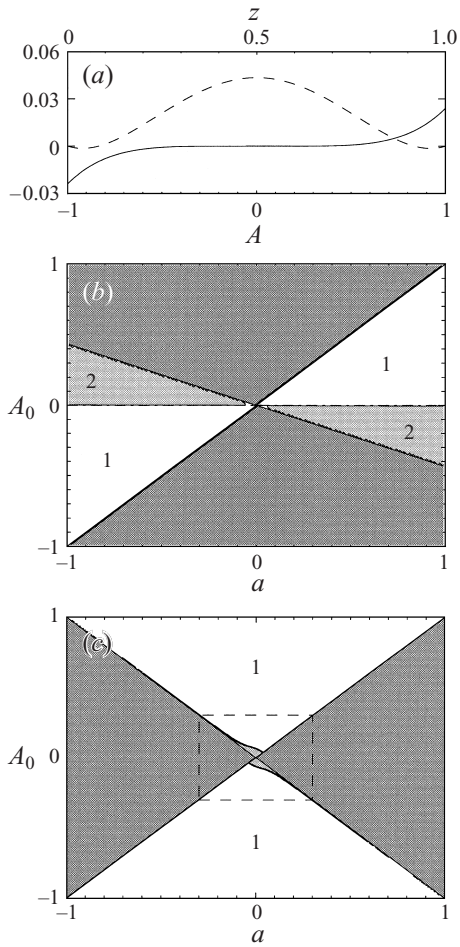


FIGURE 5. As for figures 3 and 4, except for the shear (79) and nonlinear function (80). (*b*) The characteristic diagram for positive γ, and (*c*) for negative γ. For positive γ the line of marginal stability is also the boundary between the type 1 and 2 solitary wave regions.

Integration by parts can be used to show

$$g(A) = \pi A(\bar{u}(0) + \bar{u}(1)) - \pi A \int_0^1 F_\xi \bar{u}'(\xi)\,\mathrm{d}\xi, \tag{83a}$$

where

$$F = -\frac{1}{2\pi^2}\cos 2\pi z + (2z-1)\xi - z^2 - \frac{2A}{\pi^2}\cos \pi z. \tag{83b}$$

The linear term in g can be ignored as this can be incorporated in the linear velocity of the wave; consequently it can be assumed that $\bar{u}(0) = -\bar{u}(1)$. Defining $|\bar{u}_z|_{\max} = \max(|\bar{u}_z|)$, then

$$\left| A \int_0^1 F_\xi \bar{u}'(\xi)\,\mathrm{d}\xi \right| \leqslant |\bar{u}_z|_{\max} |A(F(1) - F(0))| = |\bar{u}_z|_{\max} 4A^2, \tag{84}$$

https://doi.org/10.1017/S002211209900587X Published online by Cambridge University Press

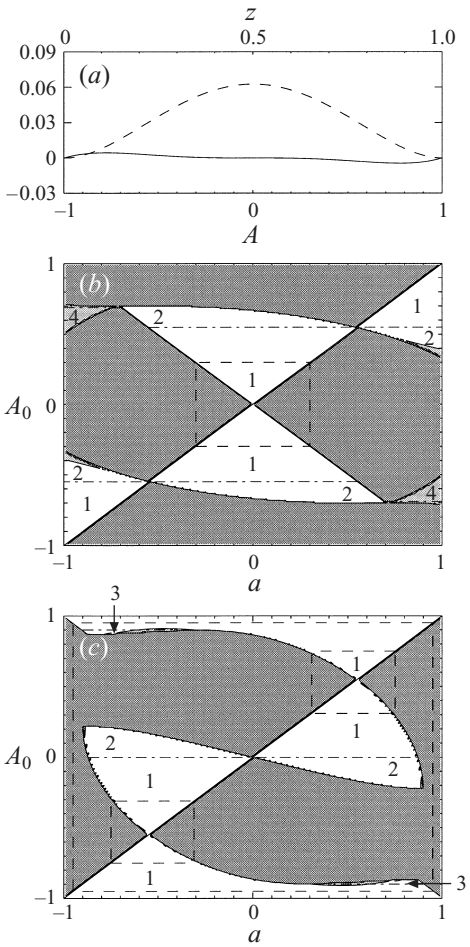


FIGURE 6. As for figure 5, except for the shear (81) and nonlinear function (82). For negative γ three different types of kink pairs can occur, examples of each of these are shown.

and therefore

$$|g|_{\max} \leqslant \frac{4}{\pi}|\bar{u}_z|_{\max}. \tag{85}$$

Thus, as noted in § 2, the perturbation expansion requires that $|\bar{u}_z| \leqslant O(1)$. The shear, and consequently g, should be normalized by $|\bar{u}_z|_{\max}$, which is equivalent, in terms of the original variables, to choosing the perturbation parameter $\epsilon = |\bar{u}_z|_{\max}$. The lengthscales of the steady waves are then

$$\lambda \sim (|g|_{\max})^{-1/2}. \tag{86}$$

When the shear is either a narrow jet or mixing layer shear approximate expressions can be obtained for g. A narrow jet can be approximated by

$$\bar{u} = D\delta(z - \xi_0), \tag{87}$$

where δ is the Dirac delta-function and $0 < \xi_0 < 1$. For example if

$$\bar{u} = \operatorname{sech}^2(z - \xi_0)/L, \tag{88}$$

https://doi.org/10.1017/S002211209900587X Published online by Cambridge University Press

the appropriate choice of D is

$$D = 2L. \tag{89}$$

For the singular shear, (87),

$$g = 2D\left(1 - (1 - A\cos\pi z)^{-2}\right)\left(\frac{\cos\pi z - A}{1 - A\cos\pi z}\right), \tag{90a}$$

where $z(A)$ is the solution of

$$\xi_0 = z - \frac{A}{\pi}\sin\pi z. \tag{90b}$$

For a mixing layer shear, i.e. a narrow transition between two regions of constant but unequal velocity, the form (83) is used for g and $\bar{u}'$ is approximated as

$$\bar{u}' = D\delta(z - \xi_0), \tag{91}$$

where $0 < \xi_0 < 1$. When

$$\bar{u} = \tanh(z - \xi_0)/L, \tag{92}$$

then $D = 2$. Ignoring the $O(A)$ terms, for the shear (91),

$$g = \frac{2AD}{\pi}\left(\frac{\sin 2z}{1 - A\cos z} + 2z\right), \tag{93a}$$

where, again, z is the solution of

$$\xi_0 = z - \frac{A}{\pi}\sin\pi z. \tag{93b}$$

For $L \geqslant O(1)$ the shears (88) and (92) both could be approximated by polynomial shear and evaluated explicitly.

In all the examples of shear considered here, and many examples not shown, no cases have been found where g has more than three inflection points. An explanation for this is that, in terms of the number of inflection points of g, shears that result in a large number of inflection points are localized in parameter space. Consequently a small perturbation to the shear can result in a significant reduction in the number of inflection points. To demonstrate this consider some special examples when the shear profile is a polynomial in z. For each positive integer k there is a unique family of polynomial shear, $\overline{U}^k$, which results in a nonlinear function $g = g_k A^k$. This nonlinearity has a multiple inflection point of order $k - 2$ at $A = 0$. Thus, by perturbing the shear profile slightly, as in proceeding from figure 3 to 4 and from figure 5 to 6, it should be possible to separate the multiple inflection point into $k - 2$ inflection points. Consider then the perturbed shear

$$\bar{u} = \overline{U}^k + \epsilon\hat{U}. \tag{94}$$

If linear shear of the form

$$\hat{U} = z - \tfrac{1}{2} \tag{95}$$

is used to perturb the shear, the resulting nonlinear function is

$$g = g_k A^k - \frac{\epsilon 4A^2}{\pi}, \tag{96}$$

https://doi.org/10.1017/S002211209900587X Published online by Cambridge University Press

which has inflection points at

$$A_j = \left| \frac{8\epsilon}{\pi g_k k(k-1)} \right|^{\frac{1}{k-2}} \exp \frac{\mathrm{i}\pi}{k-2} (\tfrac{1}{2}(1 - \operatorname{sgn} \epsilon g_k) + 2j), \quad j = 1, \ldots, k-2. \tag{97}$$

The number of real inflection points is then

$$N = 1 + \tfrac{1}{2} \left(\operatorname{sgn} \epsilon g_k + (-1)^k \right), \tag{98}$$

which results in a maximum of two inflection points for k even and ϵg_k positive. For the perturbation

$$\hat{U} = z(1-z), \tag{99}$$

the perturbed nonlinear function is

$$g = g_k A^k - \frac{\epsilon A^3}{\pi}. \tag{100}$$

This has inflection points at $A = 0$ and at

$$A_j = \left| \frac{6\epsilon}{\pi g_k k(k-1)} \right|^{\frac{1}{k-3}} \exp \frac{\mathrm{i}\pi}{k-3} (\tfrac{1}{2}(1 - \operatorname{sgn} \epsilon g_k) + 2j), \quad j = 1, \ldots, k-3. \tag{101}$$

The number of real inflection points is

$$N = 2 + \tfrac{1}{2} \left(\operatorname{sgn} \epsilon g_k - (-1)^k \right), \tag{102}$$

and the maximum number of inflection points is three for k odd and ϵg_k positive. It would be expected that more general shear profiles which result in a large number of separate inflection points are similarly unstable to perturbations. Consequently, it would appear to be sufficient to only consider here shear profiles which result in three or less inflection points. This encompasses all but a very small fraction of the cases that can occur.

All types of shear profiles support solitary waves to some degree; however only those for which the function g has an inflection point will support kinks. From the examples of shear profiles considered here it appears that a necessary condition for this to occur is that the shear has a turning point. These examples also suggest that a necessary condition for the instability of solitary waves is that the shear must have an inflection point. For example, for the shear profiles $\sin \pi z$ and $\exp -(z/L)$ the existence and stability diagrams have no regions of unstable solitary waves. This condition, however, only isolates the types of shear which cannot have unstable solitary waves, as many types of shear with inflection points also do not have regions of instability. One such example is the mixing layer shear profile considered previously.

4. Evolution of periodic waves

If $g \equiv 0$ an exact solution of (32) is any periodic wave. As noted in § 2, since the sheared current is a weak effect g can be allowed to vary with χ. Therefore, an obvious and practical problem to consider is the evolution of a periodic wave in time, such as an internal tide, propagating from a region of no shear into a region of weak shear.

For T-periodic waves (32) should be modified to have a term depending on χ on the right-hand side; however this can be neglected if it is first differentiated with

https://doi.org/10.1017/S002211209900587X Published online by Cambridge University Press

respect to θ, giving the Volterra integral equation of the second kind:

$$K(A,A)A_\chi + A_\theta \int_T^\theta K_A(A,A')A'_\chi \,\mathrm{d}\theta' + g_A A_\theta + A_{\theta\theta\theta} = 0. \tag{103}$$

This is to be solved with the initial condition

$$A(\theta,0) = \alpha \sin \frac{2\pi\theta}{T}. \tag{104}$$

To model this problem correctly, the function g should vary slowly from zero to an asymptotic value; however in practice suddenly allowing g to attain a steady-state value has little effect on the asymptotic results. The period of the wave can be chosen arbitrarily as (103) is invariant under the transformation

$$(\theta, T) \to v(\theta, T), \qquad \chi \to v^3\chi, \qquad g \to v^{-2}g. \tag{105}$$

Therefore changing the period is effectively the same as changing the strength of the shear.

Rather than considering specific shear profiles we simply consider here the function (59) for a range of the parameters $\boldsymbol{G} = (g_2, g_3, g_4, g_5)$. This has at most three inflection points at $A = A_{1,2,3}$ and can have regions of unstable solitary waves if either g_4 or g_5 are non-zero. As was outlined at the conclusion of the previous section it is anticipated that only a very small number of shear profiles will have more than three inflection points.

Thus there are five free parameters for this problem: the four components of $\boldsymbol{G}$ and α, which is too large a parameter space to investigate. First, we can limit α to the single value $\alpha = 0.3$. The exact choice of α is arbitrary; however it must be sufficiently large for nonlinear effects to be significant and sufficiently less than 1 to prevent overturning occurring rapidly. For $\alpha \ll 1$, in general the FALW equation (103) will reduce to the KdV or mKdV equation and as there is no mechanism here to cause waves to grow resonantly, weakly nonlinear waves will remain weakly nonlinear. Resonant growth of weakly nonlinear waves can occur, however, in the special case where both the quadratic and cubic coefficients of g are exactly zero. For values of $\alpha > 0.3$ overturning will occur more often, and where it already occurs, it will occur more rapidly. Secondly, only the relative values of the components of $\boldsymbol{G}$ need be considered, rather than the total magnitude. The transformation (105) and § 3 demonstrate that increasing the magnitude of g will shorten the lengthscale of the resultant waves and the timescales over which these evolve. In the unsteady problem it would therefore be expected that increasing the magnitude of g will result in more and shorter waves evolving from the initial condition. A consequence of this is that overturning will occur more often. Conversely, decreasing the magnitude of g will result in longer and fewer waves. But since the relative values of the components of $\boldsymbol{G}$ still presents a considerable parameter space, a more efficient approach is suggested by the results of § 3, which show that the types of steady waves are determined by the number and position of the inflection points of g. Therefore, as any quasi-steady waves that evolve must be closely related to the steady waves discussed in § 3, it would be expected that the evolution of a periodic initial condition is to a large extent determined by the value of α relative to the inflection points of g. This forms the rationale for the examples and analysis which follow. The nonlinearities considered here together with the corresponding first mode velocity shear are summarized in table 1.

In considering unsteady solutions of (103) one aspect of particular interest is the effect of the nonlinear kernel $K(A, A')$. One effect that can be deduced is that, for a

https://doi.org/10.1017/S002211209900587X Published online by Cambridge University Press

Figure	g	A_i	$\bar{u}$
7	$8A^2$	—	$-2\pi z$
8	$8A^3$	0	$8\pi z(z-1)$
9	$-8A^3$	0	$-8\pi z(z-1)$
10	$8A^3+4A^2$	−0.17	$\pi z(8z-9)$
11	$-8A^3+4A^2$	0.17	$-\pi z(8z-7)$
12	$8A^4$	0, 0	$\frac{3}{2}\pi^3 z^2(-2z+3)-14\pi z$
13	$8A^4-3A^2$	−0.25, 0.25	$\frac{3}{2}\pi^3 z^2(-2z+3)-\frac{53}{4}\pi z$
14	$8A^5$	0, 0, 0	$\frac{32}{3}\pi^3(z(z-1))^2+8\pi z(z-1)$
15	$-8A^5+2A^3$	−0.27, 0, 0.27	$-\frac{32}{3}\pi^3(z(z-1))^2-6\pi z(z-1)$

TABLE 1. A summary of the nonlinear functions $g(A)$ for the unsteady simulations shown in figures 7–15. A_i are the inflection points of g and $\bar{u}(z)$ are the corresponding velocity shears.

symmetric periodic initial condition such as (104) and when g is an odd function of A, the integral term introduces a symmetry breaking mechanism. To investigate this and other effects it is useful to compare the solutions with those of the equivalent gKdV equation, (53), which corresponds to $K(A,A')\equiv 1$. As noted in § 3, not only are the solitary wave solutions of this equation identical, but they also have the same stability characteristics. Solutions of the gKdV equation have the integral invariant

$$M(\chi)=\int_0^T A\,\mathrm{d}\theta, \tag{106}$$

which to the order considered here corresponds to conservation of mass. This quantity is referred to here as the wave mass. The mean level of the solution, $A_m=M/T$, is obviously also an invariant. However, these quantities are not invariants of unsteady solutions of (103), and so the evolution of either provides one useful means of comparison with solutions of the gKdV equation. As a consequence of the invariance of the mass, as shown by Prasad & Akylas (1997), shelves are generated which in the forced problem transport mass downstream from the topographic forcing. In the context of the unforced periodic problem this in effect corresponds to a wave-mean flow interaction, where the perturbation to the mean flow is $O(A_m)$.

In all the solutions presented here (103) is solved numerically using a scheme similar to that proposed by Yi & Warn (1987). The particular implementation here uses Fourier spectral methods to calculate the derivatives, a fourth-order integral equation solver and fourth-order Runge–Kutta timestepping. The functions $1/K(A,A)$ and $K_A(A,A')/K(A,A)$ are calculated *a priori* on a uniform grid and linearly interpolated when needed. Plots of the functions $K(A,A)$ and $K_A(A,A')/K(A,A)$ are shown in Rottman, Broutman & Grimshaw (1996).

4.1. *Zero inflection points*

In figure 7 an example is shown of purely quadratic nonlinearity. Qualitatively, the solution is very similar to that of the KdV equation with a periodic initial condition. The wave steepens near the crest and then the shock evolves into a fan of rank-ordered solitary waves. Initially the level these waves propagate upon decreases downstream from the leading wave and the shock is necessary to restore the level to its maximum. Asymptotically the solitary waves propagate on an almost constant level and at longer

https://doi.org/10.1017/S002211209900587X Published online by Cambridge University Press

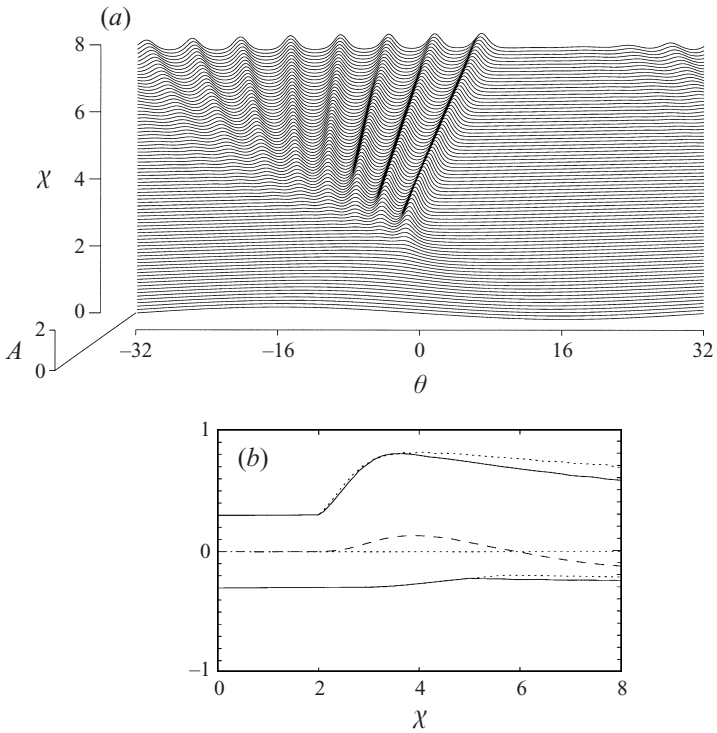


FIGURE 7. A solution of (103) and (104) with $g = 8A^2$ and $\alpha = 0.3$. (*a*) The evolution of A. (*b*) The evolution of the maximum and minimum amplitudes, shown as solid lines, and the wave mass (106), shown as a dashed line. Also shown as dotted lines are the equivalent values obtained from the solution of (53).

times than shown, since as a slow variation in the amplitude between two unequal values is not a solution of the steady equation, the level upon which the solitary waves propagate will become constant and negative. The solution at these times will simply consist of a number of interacting solitary waves. Quantitatively, there are significant differences from the KdV solution. In the FALW solution the maximum amplitude of the waves decreases significantly faster than for the KdV solution and the minimum amplitude of the waves, effectively the level upon which the waves propagate, is lower than in the KdV solution. The result of both of these effects is that in the FALW solution the speed of the individual waves is slower. As the waves are amplified it is apparent that the wave mass and mean level of the solution increases, then decreases as the waves are damped. Although the change in the wave mass clearly appears large, the maximum change in the mean level of the solution is $O(10^{-3})$.

The characteristic diagram for quadratic nonlinearity is identical to figure 3(*b*) without the regions of instability. Since the component waves are slowly varying it is useful to consider the asymptotic solution shown in figure 7 in terms of this characteristic diagram. The solution can be represented as a number of points each representing a solitary wave on a line of constant A_0, where in this case $A_0 \approx -0.2$. Then only waves with positive amplitude, i.e. $a > A_0$, form as negative amplitude, i.e. $a < A_0$, waves cannot exist.

https://doi.org/10.1017/S002211209900587X Published online by Cambridge University Press

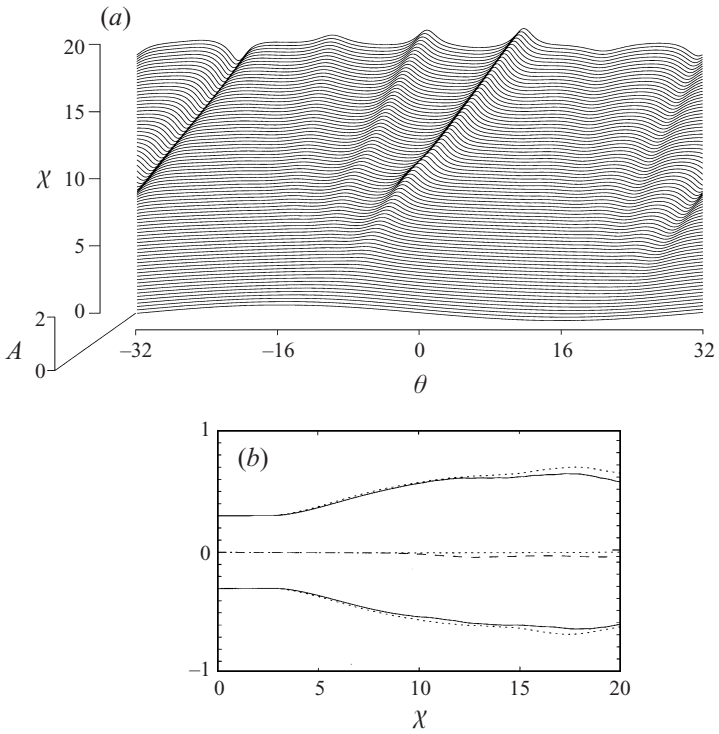


FIGURE 8. As for figure 7, except that $g = 8A^3$.

4.2. *One inflection point*

One limit when g has a single inflection point is $\alpha \gg |A_1|$, which is represented by the case of purely cubic nonlinearity. Here two completely different types of asymptotic solution occur for positive and negative cubic nonlinearity, where positive or negative refers to the sign of g_3. Examples of solutions for positive and negative cubic nonlinearity are shown in figures 8 and 9 respectively. These are qualitatively very similar to the solutions of the mKdV equations with a periodic initial condition presented by Grimshaw, Pelinovsky & Talipova (1998), except there the simulations are run to longer time allowing interactions of the waves.

In the example of positive nonlinearity shown in figure 8, the steepening occurs at the crest and trough of the wave. Each of these events evolves into a fan of solitary waves which asymptotically propagate on a constant mean level $A_m = O(10^{-3})$, where the decrease in the mean level of the solution is due the symmetry breaking effect of the nonlinear kernel. This also results in the absolute values of the maximum and minimum amplitudes in the FALW solution being always less than the corresponding values in the mKdV solution, with the consequent result that the individual waves are slower. For this nonlinearity the characteristic diagram is identical to figure 5(b) without the regions of instability. The asymptotic solution can be represented on this diagram as a number of positive and negative waves on the line $A_0 = 0$, as the inflection point is the only level at which a continuous solution can exist with both positive- and negative-amplitude waves.

For negative nonlinearity, figure 9, steepening occurs on the rear face of the crest and trough, and instead of evolving into a train of solitary waves, the shocks on each face evolve into kinks, or dispersionless shocks. These connect two plateaux of

https://doi.org/10.1017/S002211209900587X Published online by Cambridge University Press

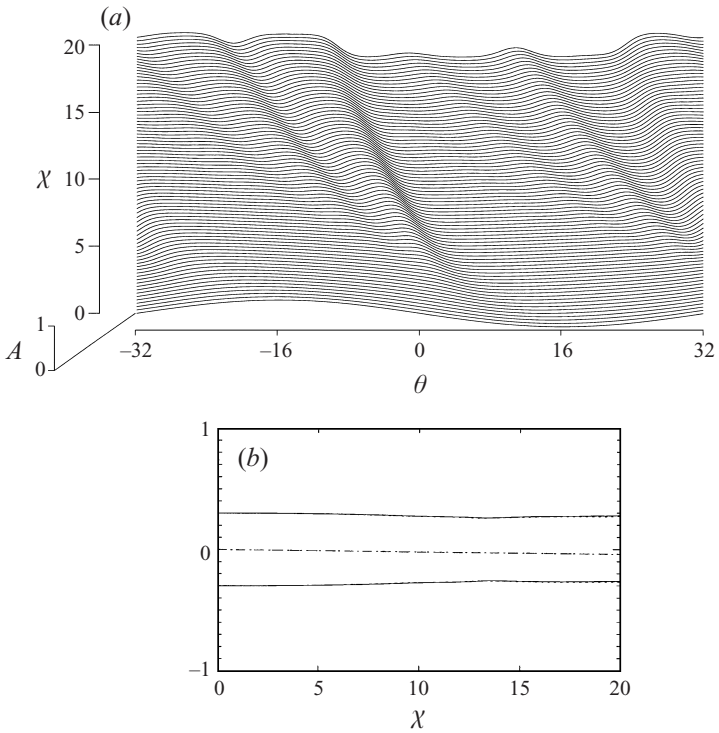


FIGURE 9. As for figure 7, except that $g = -8A^3$. In (b) the solution of the gKdV equation is almost identical, and so the comparisons are obscured.

constant, but non-zero, levels upon which solitary waves form. The levels of these plateaux are less than the initial amplitude of the wave, which contrasts with figures 7 and 8 where the amplitude increases from its initial value. Now the solution is indistinguishable from the mKdV solution. The characteristic diagram for this case is identical to figure 5(c) without the small regions of instability in the vicinity of the origiin. There are now two base levels which solitary waves propagate on, thus the asymptotic solution can be represented on the characteristic diagram on a kink pair centred about the inflection point. Negative-amplitude solitary waves form on the upper level of the kink pair and positive-amplitude solitary waves form on the lower level.

In figure 10 an example is shown when α and $|A_1|$ are of the same order of magnitude with A_1 negative. Steepening now only occurs at the crest of the wave, where initially quadratic nonlinearity dominates. At longer times cubic nonlinearity modifies the waveforms and causes the positive-amplitude waves to be preceeded by a longer negative-amplitude wave. Comparison with the gKdV solution demonstrates that the kernel limits the maximum amplitude attained in the FALW solution. Eventually the amplitude in the gKdV solution exceeds unity, which in the context of the FALW equation we take to indicate that overturning is incipient. However, this does not occur in the FALW solution, but rather the amplitude slowly decreases after attaining its maximum. This period is characterized by a decrease in the wave mass and mean amplitude. As a result of the decrease in maximum amplitude, the relative speeds of the waves are significantly less in the FALW solution. The characteristic diagram for this case is similar to figure 5(b), again without the regions of instability, but with the

https://doi.org/10.1017/S002211209900587X Published online by Cambridge University Press

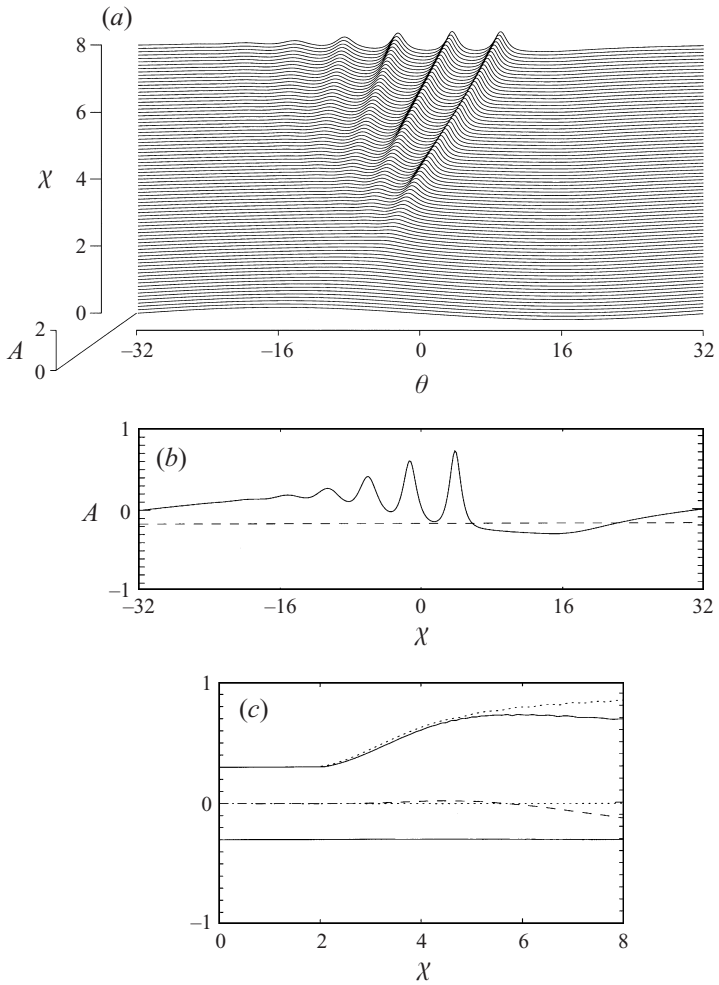


FIGURE 10. A solution of (103) and (104) with $g = 8A^3 + 4A^2$ and $\alpha = 0.3$. (*a*) The evolution of A. (*b*) The amplitude at $\chi = 8$ with the level of the inflection point of g is shown as a dashed line. (*c*) The evolution of the maximum and minimum amplitudes, shown as solid lines, and the wave mass, (106), shown as a dashed line. Also shown as dotted lines are the equivalent values obtained from the solution of (53).

whole diagram translated along the line $a = A_0$. Now it is clear that the only level that a continuous solution can exist with positive- and negative-amplitude waves is if the level that solitary waves propagate on is that of the inflection point $A_0 = A_1$. This level, which is not necessarily equal to the mean level, we refer to as the controlling level of the solution.

For positive A_1, figure 11, the effect of cubic nonlinearity is again only dominant for large times. Initially quadratic nonlinearity causes the crest of the wave to steepen and then cubic nonlinearity modifies the behaviour. Two dispersionless shocks evolve from the initial shock, a large shock at the front and a smaller shock downstream of this. Downstream of this rear shock the waves propagate on a slowly decreasing level until the upstream shock restores the level. It is apparent from figure 11(*a*) that the height of the rear shock increases with time; at large times it would be expected that this will have the same height as the forward shock and the mean level of the

https://doi.org/10.1017/S002211209900587X Published online by Cambridge University Press

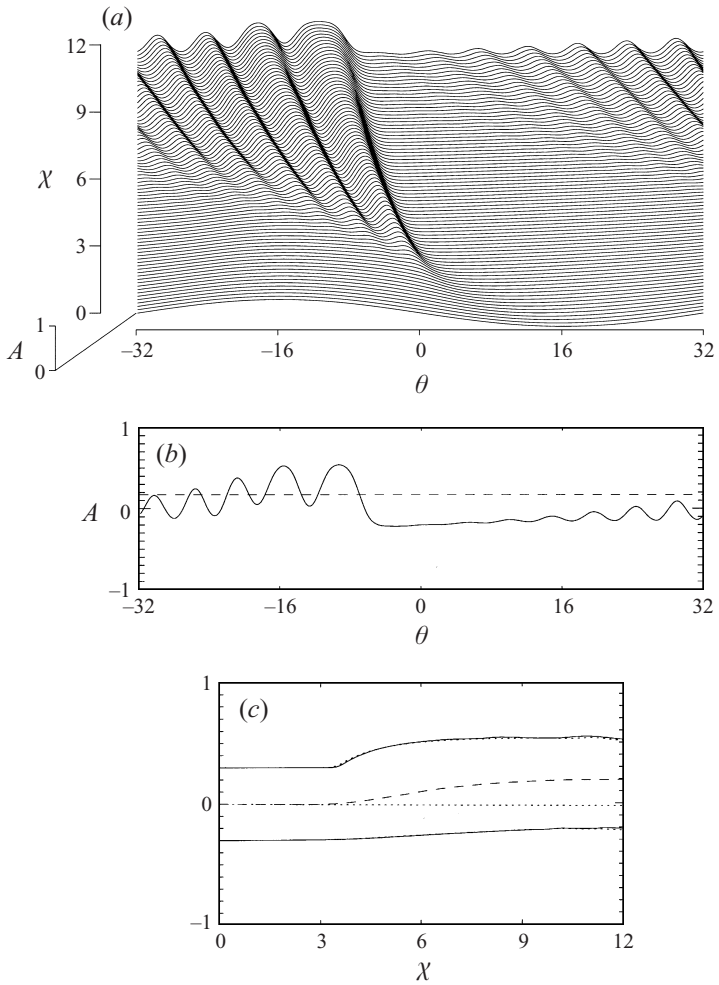


FIGURE 11. As for figure 10 except $g = -8A^3 + 4A^2$ and the solution in (b) is shown at $\chi = 12$.

lower plateau will be approximately constant. This must be the case as otherwise the mean level would be slowly varying, which cannot be a solution of (103). The solution will then consist of two plateaux upon which a number of interacting solitary waves propagate. The levels of these plateaux are then equidistant from the level of the inflection point A_1, as is apparent from figure 11(b, c). The comparison with the gKdV solution in figure 11(b), shows that although the maximum and minimum amplitudes are almost identical, there is a significant increase in the wave mass. The characteristic diagram for this case is identical to figure 5(c) without the regions of instability and translated along the line $a = A_0$. Again, consideration of the asymptotic solution in terms of the characteristic diagram clearly demonstrates that the inflection point is the controlling level of the solution.

Consider then the asymptotic behaviour as the inflection point of g moves out from $A = 0$ to $A = \pm 1$. If the characteristic solution at $A_1 = 0$ is one of positive and negative solitary waves propagating on the controlling level of the inflection point, as in figures 8 and 10, then as the inflection point moves away from the origin the asymptotic solution becomes more asymmetric about the inflection point, with the

https://doi.org/10.1017/S002211209900587X Published online by Cambridge University Press

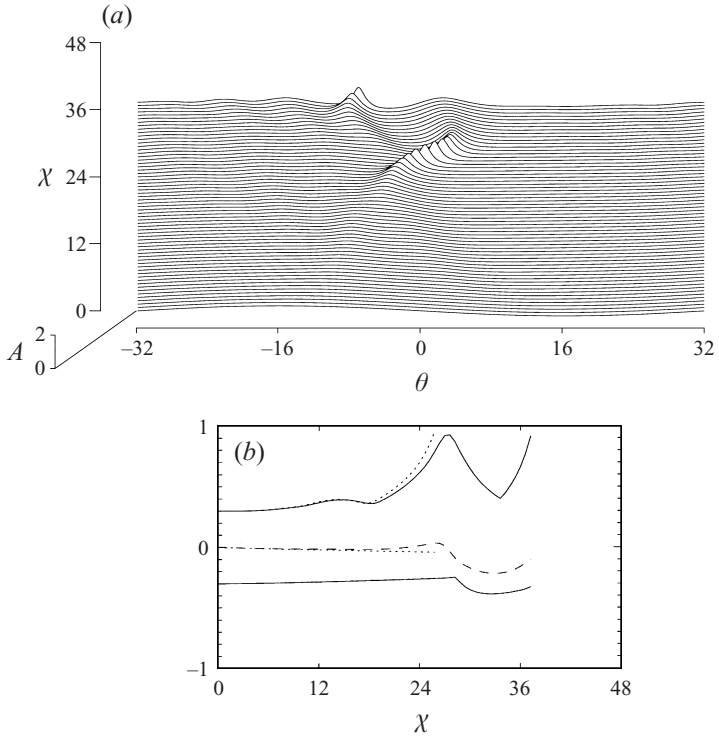


FIGURE 12. As for figure 8 except $g = 8A^4$. The simulation of (103) is stopped at $\chi \approx 37$ due to overturning.

larger-amplitude waves facing toward $-\mathrm{sgn}\,(A_1)$. Eventually only positive or negative solitary waves propagate on the controlling level. Then as the inflection point moves further away from the origin the asymptotic solution is no longer controlled by the inflection point. Rather a train of rank-ordered solitary waves form propagating on a mean level as in figure 7. This type of solution would be expected to occur for $\alpha \gg |A_1|$. If the asymptotic solution at $A_1 = 0$ consists of solitary waves propagating on a kink pair, as in figures 9 and 11, then as the inflection point moves away from the origin the length of the plateaux becomes asymmetric with the longer plateau being closer to the origin. Before the amplitude of this longer plateau approaches zero, the length of the shorter plateau must decrease to zero, at $\alpha \sim |A_1|$. Then as the inflection point moves further away from the origin it is no longer the controlling level of the solution, instead rank-ordered solitary wave solutions such as those in figure 7 form.

4.3. *Two inflection points*

When the absolute value of either A_1 or A_2 is significantly larger than α the solutions need not be considered in detail here. When both are significantly larger the behaviour will be similar to that shown in figure 7, while when one is significantly larger the behaviour will be qualitatively the same as shown in figures 8–11.

Consider first the limiting case of purely quartic nonlinearity. This has a double inflection point at the origin which introduces a region of unstable solitary waves on the relevant characteristic diagram, figure 3(*b*). In the example shown in figure 12 it is the effect of this unstable region that is of particular interest, as the solitary

https://doi.org/10.1017/S002211209900587X Published online by Cambridge University Press

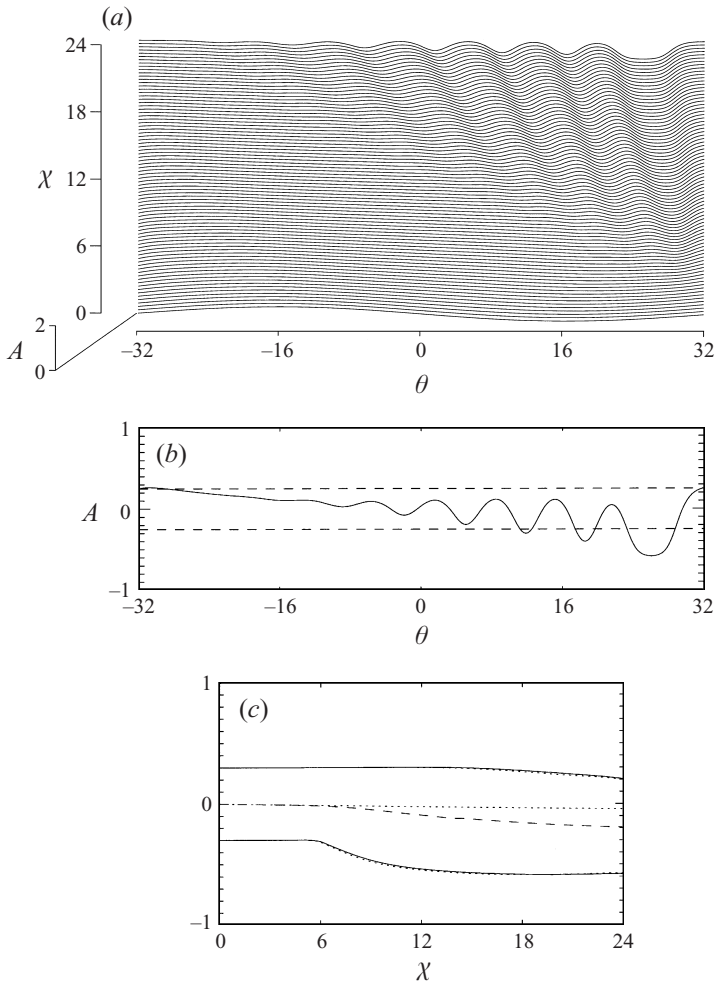


FIGURE 13. As for figure 10 except $g = 8A^4 - 3A^2$ and here the solution in (*b*) is shown at $\chi = 24$ and there are two inflection points.

waves which form have amplitudes falling in this region. In the context of the gKdV equation this instability leads to critical collapse, or the formation of a singularity. The gKdV simulation is halted at $\chi \approx 24$ as due to this instability the amplitude exceeds unity. Initially for the FALW equation the behaviour of the solitary wave is the same; however, as has been seen in previous cases, as the amplitude increases the nonlinear kernel damps the growth of the solitary wave. Eventually for the leading solitary wave this leads to its collapse into a smaller-amplitude stable solitary wave and trailing radiation. However, the leading wave of this radiation becomes unstable and eventually the amplitude exceeds unity, indicating that overturning may occur. As can be seen this critical collapse and decay causes a significant variation in the wave mass.

If either A_1 or A_2 is non-zero then the characteristic diagram will be of type shown in figure 4(*b*). Thus if $|A_1| \sim |A_2| \sim \alpha$, but the two inflection points are of opposite sign, it would be anticipated that the periodic initial condition could evolve to one of two asymptotic solutions. One possibility is that the upper inflection point is the

https://doi.org/10.1017/S002211209900587X Published online by Cambridge University Press

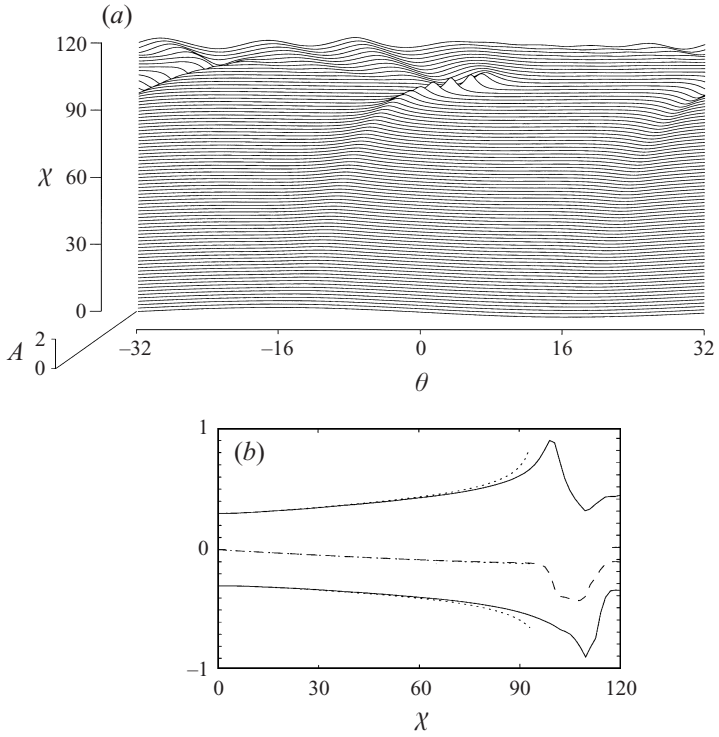


FIGURE 14. As for figure 8 except $g = 8A^5$.

controlling level of the solution, in which case a solution with positive and negative solitary waves propagating on the level of the inflection point would be expected to form. The other possibility is that the lower inflection point is the controlling level, in which case the asymptotic solution will consist of a kink pair centred about the inflection point, with solitary waves propogating on the two plateaux separating the kinks. In figure 13 an example is shown where $A_1 = -A_2$. As is apparent a kink pair solution centred about the lower inflection point forms and the upper inflection point has little effect. Let A_1 be the lower inflection point and A_2 the upper inflection point. Then, other simulations not shown here for which $A_2 < -A_1$ show that the kink pair configuration still forms preferentially. Thus the kink pair configuration appears to be considerably more stable than the configuration of positive and negative solitary waves propagating on the level of an inflection point.

4.4. *Three inflection points*

Again, if any of the inflection points $A_{1,2,3}$ is significantly larger than α it would be expected that the behaviour would be similar to that described above. The examples which follow describe two unique types of solution which can occur when there are three inflection points.

Consider first the case of purely quintic nonlinearity, for which the characteristic diagram is figure 6(b,c). As for cubic nonlinearity, the behaviour is dependent on the sign of the nonlinear coefficient. For positive nonlinearity, as well as the inflection point at $A = 0$ there is a large region of unstable solitary waves, which as shown by Pelinovsky & Grimshaw (1997) includes the line $A_0 = 0$. An example of positive quintic nonlinearity is shown in figure 14. The asymmetry caused by the nonlinear

https://doi.org/10.1017/S002211209900587X Published online by Cambridge University Press

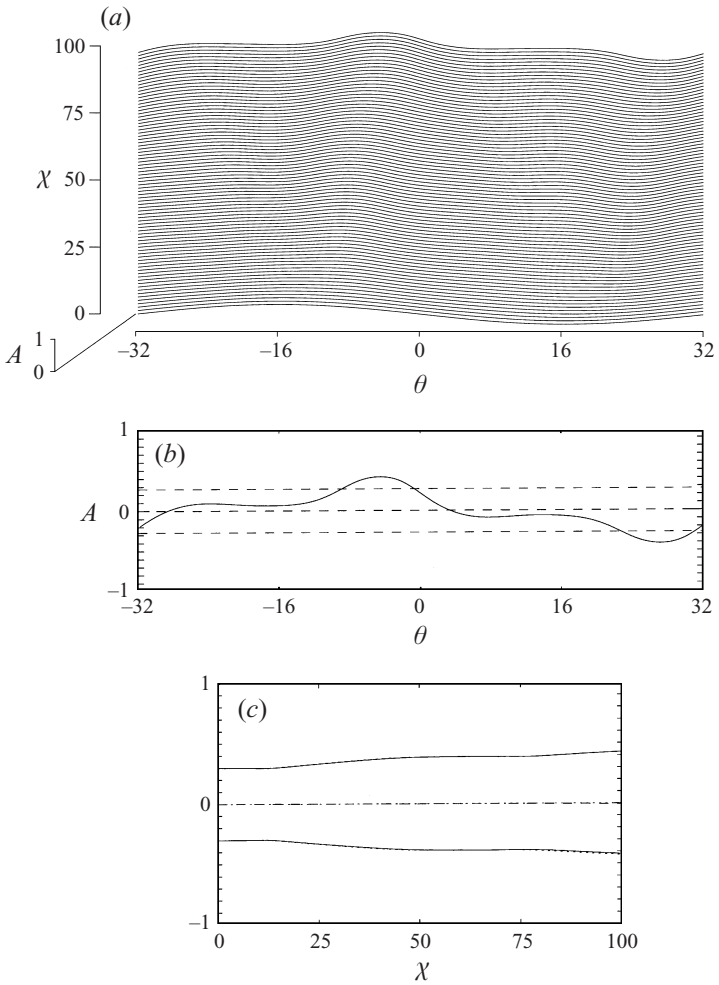


FIGURE 15. As for figure 10 except $g = 8A^5 + 2A^3$ and here the solution in (b) is at $\chi = 100$ and there are three inflection points.

kernel can clearly be observed in this case. As with figure 12 in the gKdV solution the solitary wave instability leads to the formation of a singularity; here the simulation is stopped at $\chi \approx 90$ due to the amplitude exceeding unity. However, the nonlinear kernel again halts this critical collapse causing the unstable solitary waves to decay into radiation. It is anticipated that the largest of these waves will become unstable and the process of amplification and decay of the waves will continue. As can be seen in figure 14(b) the wave mass has a sudden decrease due to the decay of the first unstable solitary wave and then increases with the decay of the second unstable solitary wave.

In figure 15 an example is shown where A_1 and A_3 are of opposite sign and $A_2 = 0$. In this case the characteristic diagram is similar to figure 6(b), for which three levels of kink pairs are possible. With three, unique inflection points a kink triplet solution is possible. Here, the upper and lower levels are considerably shorter than the central level. A representation of the solution on the characteristic diagram reveals that this kink triplet solution is the limit of solutions such as that shown in figure 8, where the

https://doi.org/10.1017/S002211209900587X Published online by Cambridge University Press

largest positive- and negative-amplitude solitary waves have each become a kink pair. As the two outer inflection points move closer to the origin these kink pairs would be expected to increase in length until the central level disappears. Then in this limit the solution will be qualitatively similar to figure 9.

5. Comparison with observations

A general comparison of the results of the previous section can now be made with the data from the Australian North West Shelf presented in Holloway (1984, 1987) and Smyth & Holloway (1988). We will confine our comments to the data and analysis presented in the latter. This shows the time series for an internal tide propagating onto a shelf break, together with the ambient stratification and shear. These are such that the fluid is approximately linearly stratified and the shear is weak, while the internal tide is of finite amplitude. Indeed the waves have amplitude of $O(40\,\mathrm{m})$ in fluid of depth $O(120\,\mathrm{m})$, which is slightly greater than the overturning amplitude for the theory presented herein. The measurements were made at two points, at North Rankin in fluid of depth $O(120\,\mathrm{m})$ and further up the shelf at Mooring 5 in fluid of depth $O(70\,\mathrm{m})$. These measuring stations fall in regions of slowly varying depth, separated by a sudden decrease in the depth of the fluid. Thus, as a first approximation it can be assumed that in the vicinity of each of the measuring stations the depth, shear and stratification were approximately constant. Two data sets were presented from each of the measuring stations. Smyth & Holloway (1988) stated that from those data the characteristic behaviour was that as the internal tide propagates up the shelf it forms into shocks or hydraulic jumps. A summary of the shock and solitary wave formation at both measuring stations is presented in table 2. Also shown is a calculation of the coefficients and inflection points for the nonlinear function $g(A)$ for this data.

Consider the data set NR/1, which has no inflection points. The characteristic solution for the evolution of the internal tide in this case should be that the wave steepens and forms into a train of rank-ordered solitary waves. As is apparent, this appears to be what occurs. In the other three cases there is one positive inflection point and the quadratic nonlinear coefficient, g_2, is also positive. Thus the characteristic asymptotic solution should be a kink pair joining two plateaux of approximately constant level. Note that if g_2 were negative the asymptotic solution should be a train of rank-ordered solitary waves again. The evolution of the two kinks should be governed by differing timescales. The leading kink forms from steepening governed by quadratic nonlinearity, thus there should be a number of solitary waves immediately downstream of the kink, whereas the evolution of the rear kink is governed by cubic nonlinearity, and so is largely dispersionless. These general features of the solution are in concurrence with all of the last three data sets in table 2.

6. Conclusions

The propagation of finite-amplitude long internal waves in uniform stratification and with weak shear has been considered here. It has been shown that the inclusion of shear introduces a nonlinear term to the finite-amplitude long-wave equation. This nonlinear term is an amplitude representation of the physical shear profile in z-space. Boussinesq effects have been ignored here; their inclusion would introduce a further nonlinear term of the form shown by Grimshaw & Yi (1991). The magnitude of the ratio of the nonlinear term due to velocity shear and the term due to Boussinesq

https://doi.org/10.1017/S002211209900587X Published online by Cambridge University Press

Data Set	$g_4 : g_3 : g_2$	A_i	Comments
NR/1	0.28 : −0.75 : 1	—	4 forward breaking shocks. No rearward shocks, but some steepening on rear face of wave. Large amplitudes form on front shock.
NR/2	0.26 : −0.99 : 1	0.44	12 forward facing shocks and 5 rearward facing shocks. In other cases some steepening on rear face. A few large-amplitude waves on front shocks.
M5/1	0 : −0.81 : 1	0.41	6 forward facing shocks and 5 rearward facing shocks. High frequency, small amplitude waves on front shocks.
M5/2	0 : −1 : 0.45	0.15	11 forward facing shocks and 8 rearward facing shocks. A few large-amplitude waves on front shocks.

TABLE 2. A summary of the observations of solitary wave and shock formation taken from the isopycnal displacements of figure 3 of Smyth & Holloway (1988). The North Rankin (NR) measurements were taken in water of depth 120 m and the Mooring 5 (M5) in depth 67 m. Data Set 1 of each was taken over the interval 2 to 5 March, 1982 and Data Set 2 over the interval 28 March to 3 April, 1982. The parameters $g_4 : g_3 : g_2$ were calculated using the corresponding shear profiles from figure 2 of Smyth & Holloway (1988). A polynomial was fitted to these points and used in (59) to calculate the normalized nonlinear coefficients, where the normalization preserves the sign of the coefficients. These were then used to calculate the inflection point A_i. For all the shear profiles no regions of unstable solitary waves were found.

effects is then

$$\frac{\Delta\rho}{\rho}(Ri^{1/2})_{\min}, \tag{107}$$

where Ri is the Richardson number of the undisturbed fluid. Typically $\Delta\rho/\rho < 10^{-3}$, therefore the shear need not be particularly strong before it dominates Boussinesq effects.

When the waves are steady the FALW equation reduces to the steady form of the gKdV equation which can be conveniently analysed to determine the possible types of solitary waves and their stability. It is found that the types of solitary waves which occur depend upon the inflection points of the nonlinear function $g(A)$. If g has no inflection points only subexponential solitary waves are possible. These correspond to solitary waves with only one characteristic lengthscale. When g has one or more inflection points superexponential solitary waves and kinks are also possible. These superexponential waves then can have more than one characteristic lengthscale, and appear to only be able to occur when the shear profile has a turning point. As the complexity of the shear or number of inflection points of g increases, the size of the regions in which solitary waves are unstable increases. The function g and the regimes in which each of these types of solitary waves occur have been presented for various shear profiles. Significantly, it has been found that unstable solitary waves only occur if the shear has an inflection point.

A theory based on the inflection points of g rather than its order is of much more general applicability. For example, for all types of shear profiles with an exponential behaviour in z the function g can only be obtained by numerical integration. These integrations, which are not shown here, demonstrate that for all such shear profiles g

https://doi.org/10.1017/S002211209900587X Published online by Cambridge University Press

appears to have no inflection points. Hence, only the first type of solitary waves are possible and the kinematic effect of these exponential shears could be approximated by a linear velocity shear. From the examples considered here and others not shown it may be that for any shear the amplitude representation g will have at most three distinct inflection points.

The evolution of a periodic initial condition has been presented for various $g(A)$. Two asymptotic types of solution have been found, where in general the type of solution is again dependent on the inflection points of g and the behaviour of g in the limit $A \to 0$. For the first type of solution the periodic wave forms into a shock, which then evolves into a train of rank-ordered solitary waves propagating on a non-zero mean level. In the second type of solution an initial shock forms into two or more kinks connecting two or more plateaux. Solitary waves propagate on these plateaux. These two types of solutions can be used to explain the observations of shock formation reported in Holloway (1984, 1987) and Smyth & Holloway (1988). All the solutions suggest that when the amplitude of the waves becomes large there is a significant transfer of mass between the waves and the mean flow. Consequently, in this limit the effect of current shear is no longer purely kinematic. This wave–mean flow interaction requires further research.

Recently Holloway *et al.* (1997) used a weakly nonlinear gKdV equation incorporating horizontal variability and bottom friction to model the internal tide data from the Australian North West Shelf presented in Holloway (1994). They found that the horizontal variability can cause the coefficient of the (quadratic) nonlinear term to change sign and this plays an important part in determining the evolution of the internal tide. The inclusion of bottom friction was also found to be significant in that it limited the wave amplitudes. The theory presented here cannot be applied to these data as the stratification is not uniform and almost all the datasets show large regions of overturning. The results of Holloway *et al.* (1997) do however suggest possible important extensions to the FALW equation presented here. The inclusion of bottom friction would be especially significant in preventing overturning in many cases and the gradual change in depth must introduce a further term to the FALW equation and result in the modulation of the nonlinear function $g(A)$.

This work was supported by the Australian Research Council. Sincere thanks are due to Professor Jörg Imberger who initially supported and suggested this topic while S. R. C. was at the Centre for Water Research, University of Western Australia.

REFERENCES

Apel, J. R., Byrne, H. M., Proni, J. R. & Charnell, R. L. 1975 Observations of oceanic internal and surface waves from the Earth Resources Technology Satellite. *J. Geophys. Res.* **80**, 865–881.

Benney, D. J. 1966 Long nonlinear waves in fluid flows. *J. Maths and Phys.* **45**, 52–63.

Benney, D. J. 1979 Large amplitude solitary Rossby waves. *Stud. Appl. Maths* **60**, 1–10.

Benney, D. J. & Ko, D. R. S. 1978 The propagation of long large amplitude internal waves. *Stud. Appl. Maths* **59**, 187–199.

Derzho, O. & Grimshaw, R. 1997 Solitary waves with a vortex core in a shallow layer of stratified fluid. *Phys. Fluids* **9**, 3378–3385.

Dubreil-Jacotin, M. L. 1937 Sur les théorèms d'existence relatifs aux ondes permanentes périodiques à deux dimensions les liquides hétérogènes. *J. Math Pures Appl.* **16**, 43–67.

Farmer, D. M. 1978 Observations on long nonlinear internal waves in a lake. *J. Phys. Oceanogr.* **8**, 63–73.

Farmer, D. M. & Smith, J. D. 1978 Nonlinear internal waves in a fjord. In *Hydrodynamics of Estuaries and Fjords* (ed. J. Nihoul). Elsevier.

https://doi.org/10.1017/S002211209900587X Published online by Cambridge University Press

Gear, J. A. & Grimshaw, R. 1983 A second-order theory for solitary waves in shallow fluids. *Phys. Fluids* **26**, 14–29.

Grimshaw, R. 1981 Evolution equations for long nonlinear waves in stratified shear flows. *Stud. Appl. Maths* **65**, 159–188.

Grimshaw, R. 1997 Internal solitary waves. In *Advances in Coastal and Ocean Engineering* (ed. P. L.-F. Liu), vol. 3, pp. 1–30. World Scientific.

Grimshaw, R. H. J., Pelinovsky, E. & Talipova, T. 1998 The modified Korteweg-de Vries equation in the theory of large-amplitude internal waves. *Nonlinear Processes Geophys.* (to appear).

Grimshaw, R. & Yi, Z. 1990 Finite-amplitude long waves on coastal currents. *J. Phys. Oceanogr.* **20**, 3–18.

Grimshaw, R. & Yi, Z. 1991 Resonant generation of finite-amplitude waves by the flow of a uniformly stratified fluid over topography. *J. Fluid Mech.* **229**, 603–628.

Grimshaw, R. & Yi, Z. 1993*a* Resonant generation of finite-amplitude waves by flow past topography on a β-plane. *Stud. Appl. Maths* **88**, 89–112.

Grimshaw, R. & Yi, Z. 1993*b* Resonant generation of finite-amplitude waves by the uniform flow of a uniformly rotating fluid past an obstacle. *Mathematika* **40**, 30–50.

Halpern, D. 1971 Observations on short period internal waves in Massachusetts Bay. *J. Mar. Res.* **29**, 116–132.

Haury, L. R., Briscoe, M. G. & Orr, M. H. 1979 Tidally generated internal wave packets in Massachusetts Bay. *Nature* **278**, 312–317.

Holloway, P. E. 1984 On the semi-diurnal tide at a shelf-break region on the Australian North West Shelf. *J. Phys. Oceanogr.* **14**, 1787–1799.

Holloway, P. E. 1987 Internal hydraulic jumps and solitons at a shelf-break on the Australian North West Shelf. *J. Geophys. Res.* **92**, 5405–5416.

Holloway, P. E. 1994 Observations of internal tide propagation on the Australian North West Shelf. *J. Phys. Oceanogr.* **24**, 81–106.

Holloway, P. E., Pelinovsky, E., Talipova, T. & Barnes, B. 1997 A nonlinear model of internal tide transformation on the Australian North West Shelf. *J. Phys. Oceanogr.* **27**, 871–896.

Kakutani, Y. & Yamasaki, N. 1978 Solitary waves on a two-layer fluid. *J. Phys. Soc. Japan* **45**, 674–679.

Lee, C.-Y. & Beardsley, R. C. 1974 The generation of long nonlinear internal waves in a weakly stratified shear flow. *J. Geophys. Res.* **79**, 453–.

Long, R. R. 1953 Some aspects of the flow of a stratified fluid. I. A theoretical investigation. *Tellus* **5**, 42–57.

Maslowe, S. A. & Redekopp, L. G. 1980 Long nonlinear waves in stratified shear flows. *J. Fluid Mech.* **101**, 321–348.

Miles, J. W. 1979 On internal solitary waves. *Tellus* **31**, 456–462.

Pelinovsky, D. E. & Grimshaw, R. H. J. 1996 An asymptotic approach to solitary wave instability and critical collapse in long-wave KdV-type evolution equations. *Physica* D **98**, 139–155.

Pelinovsky, D. E. & Grimshaw, R. H. J. 1997 Instability analysis of internal solitary waves in a nearly uniformly stratified fluid. *Phys. Fluids* **9**, 3343–3352.

Prasad, D. & Akylas, T. R. 1997 On the generation of shelves by long nonlinear waves in stratified flows. *J. Fluid Mech.* **346**, 345–362.

Rottman, J. W., Broutman, D. & Grimshaw, R. 1996 Numerical simulations of uniformly stratified fluid flow over topography. *J. Fluid Mech.* **306**, 1–30.

Smyth, N. F. & Holloway, P. E. 1988 Hydraulic jump and undular bore formation on a shelf break. *J. Phys. Oceanogr.* **18**, 947–962.

Tung, K.-K., Ko, D. R. S. & Chang, J. J. 1981 Weakly nonlinear internal waves in shear. *Stud. Appl. Maths* **65**, 189–221.

Warn, T. 1983 The evolution of finite amplitude solitary Rossby waves on a weak shear. *Stud. Appl. Maths* **69**, 127–133.

Yi, Z. & Warn, T. 1987 A numerical method for solving the evolution equation of solitary Rossby waves on weak shear. *Adv. Atmos. Sci.* **4**, 43–54.

https://doi.org/10.1017/S002211209900587X Published online by Cambridge University Press